Master of Science Thesis

Production of ^{89}Zr for labelling of antibodies to be evaluated preclinically with micro-PET for radioimmunodiagnostics of prostate cancer

Christoffer Svensson

Supervisors: Tomas Ohlsson, Sven-Erik Strand and Anders Sandell

Medical Radiation Physics
Clinical Sciences, Lund
Lund University, 2008

Visualisering av prostatacancer

Prostatacancer är den vanligaste cancersjukdomen bland män i Sverige och drabbar framförallt äldre. Eftersom sjukdomsförloppet normalt sett är långsamt hinner de flesta män avlida av någon helt annan sjukdom eller orsak. Dock finns där en grupp av män som drabbas av en betydligt aggressivare form av prostatacancer som i ett tidigt skede börjar sprida sig från prostatan till övriga delar av kroppen. En tidig diagnos av sjukdomen är därför av stor betydelse för att rätt behandling ska kunnas sättas in vilket ger ökad möjlighet att tillfriskna.

Med *radioimmunodiagnostik*, d.v.s genom att koppla en *radionuklid* (radioaktivt ämne) till speciellt anpassade antikroppar mot prostata, öppnas möjligheten för att studera fördelningen av prostatacancern i kroppen. I *positronemissionstomografi* (PET) låter man det radioaktiva ämnet generera informationen till bilden. Antikropparna agerar sedan som målsökare mot de proteiner som är kopplade till prostatan. På så vis kan alltså dessa antikroppar transportera radionukliden till dessa proteiner och således visualiseras oberoende av var de befinner sig i kroppen. För att radionukliden skall vara väl lämpad för radioimmunodiagnostik med PET måste den uppfylla vissa fysikaliska krav som krävs för antikropparnas fördelning i kroppen och för goda bildgivande egenskaper. Dessutom bör produktionen vara enkel och billig samtidigt som en märkningsmetod mot antikroppen måste existera.

Zirkonium-89 (^{89}Zr) är en metallisk radionuklid som uppfyller de flesta av dessa krav. Den produceras genom att bombardera en tunn folie av yttrium med protoner från en accelerator (*cyclotron*). ^{89}Zr måste därefter separeras från yttriumfolien för att inte påverka själva märkningen mot antikroppen. Efter att den bombarderade folien lösts upp i saltsyra, görs separationen av ^{89}Zr på kemisk väg genom en speciell *jonbytarkolonn*. ^{89}Zr återfås då i en kemisk lösning. Man placerar sedan ^{89}Zr i en modifierad molekylstruktur till vilken man kopplar sin antikropp. Den typ av molekylstruktur som används kallas för *kelat*. Kelat har förmågan att binda in metalliska ämnen till organiska molekyler i en ringformad struktur. Till kelatet byggs sedan en länk som möjliggör kopplingen till antikroppen.

I detta arbete har ^{89}Zr producerats och därefter separerats till över 83 % av den ursprungliga radioaktiviteten. Försök har gjorts att koppla antikroppar till denna speciella molekylstruktur i vilken ^{89}Zr skall ingå. Även om vägen till kliniska försök fortfarande är lång är idén i allra högsta grad levande.

Abstract

Introduction: Prostate cancer is the most common cancer type among men in Sweden. The malignant growth is normally a slow process and most patients are diagnosed at an age of 70 or more. However, some are subjected to a more aggressive form that requires an early diagnose to enhance the chances to overcome the disease. By combining monoclonal antibodies (mAbs) against two proteins connected with prostate (PSA and hK2) together with positron emission tomography (PET), the diagnostics of prostate cancer could be improved. ^{89}Zr has found to fulfil several requirements to be used in immuno-PET. This thesis will describe the production, separation and conjugation of ^{89}Zr to mAbs. The imaging characteristics of ^{89}Zr compared to ^{18}F will be evaluated as well. ***Material and Methods:*** ^{89}Zr has been produced in a cyclotron (Scanditronix MC16) through ^{89}Y(p,n)^{89}Zr reactions and verified with γ-spectroscopy. The separation chemistry is based on the use of a hydroxamate column, where Zr is able to form complexes with the resin at >1M HCl, whereas Y and other impurities are not. Zr is then transchelated into 1M oxalic acid and returns as Zr oxalate. Attempts to conjugate ^{89}Zr to Rituximab with the bifunctional chelate desferrioxamine B (Desferal, Novartis) were carried out. The premodification of Df during Fe blockage enables conjugation to the mAb. After removement of Fe, ^{89}Zr can be complexed into Df. Imaging characteristics were evaluated through spatial resolution, sensitivity and scatter contribution measurements in a MicroPET Focus 120 and GE 4096 *Plus.* ***Results:*** γ-spectroscopy confirmed the production of ^{89}Zr. Except ^{89m}Zr and ^{88}Zr, no other co-produced radionuclidic impurities were revealed. Four separations of ^{89}Zr resulted in radiochemical yields ≥83 %. A spatial resolution loss of 0.4 mm was measured for ^{89}Zr compared to ^{18}F in the MicroPET Focus 120 and almost no differences were seen in sensitivity or scatter contribution in the GE 4096 *Plus.* ***Conclusions:*** Production and separation was successful even though further investigations regarding purity are needed. The conjugation method is promising but extra experiments are required. In addition, good imaging characteristics of ^{89}Zr gives good hope for immuno-PET in prostate cancer.

Keywords: prostate cancer, ^{89}Zr, hydroxamate column, desferal

Acknowledgements

My thanks go primary to my supervisors Tomas Ohlsson, Sven-Erik Strand and Anders Sandell for making this MSc thesis possible.

I would like to thank Jonathan Siikanen for his support, discussions and for sharing his office.

Special thanks to Gerard Visser and Maria Vosjan (Radionuclide Center, VU University medical center, Amsterdam) for their kindness and generosity when demonstrating the conjugation method.

To Henrik Hussein El-Ali (Panum Institute, University of Copenhagen) for helping me out with phantom studies at the MicroPET Focus 120.

David Ulmert for valuable discussions and your revision on the part concerning prostate cancer.

Thanks to Carl Östlund for his support on γ-spectroscopy with the HPGe-detector.

Gertie Johansson for her tips and tricks in the laboratory.

Tommy Jaldérus for driving me to Copenhagen early in the morning.

Jan Pallon and staff (Nuclear Physics Department, Lund University) for PIXE analysis.

Finally, to Mikael Peterson for his fruitful discussions.

Contents

Abbreviations

Df	desferal
EDC	1-(3-Dimethylaminopropyl)-3-ethylcarbodiimide hydrochloride
EOB	end of bombardment
FBP	filtered backprojection
hK2	human kallikrein 2
HPLC	high-performance liquid chromatography
LOR	line of response
mAb	monoclonal antibody
MAP	maximum a posteriori
MDP	methylene-diphosphonate
MeCN	acetonitrile
MeOH	methanol
NaOH	sodium hydroxide
PCa	prostate cancer
PET	positron emission tomography
PIXE	particle induced X-ray emission
PSA	prostate-specific antigen
RIT	radioimmunotherapy
ROI	region of interest
SPECT	single photonemission computed tomography
TFP	2,3,5,6-Tetraflurophenol

1 Introduction

The combination of the high sensitivity and good spatial resolution of positron emission tomography (PET) with the specificity of monoclonal antibodies (mAbs), so called immuno-PET, is a promising candidate in the development of diagnostic tools of cancer. There also are the possibilities of radioimmunotherapy (RIT) if high tumour-to-normal tissue activity ratios can be achieved. In the sense of diagnostics, not only to reveal the disease, but also the ability in staging and following the disease makes this technique a promising research area [1]. In comparison with the in clinic accepted as the golden standard in oncological imaging, namely FDG-PET [2], immuno-PET is different on the grounds of possible combination of tumour detection and quantification for tumour planning and therapy [3]. The introduction of small animal PET shows several advantages in the preclinical trials of drug development. For instance to determine biological properties of proteins one wants to investigate. Traditionally, samples of blood volume or tissues are often measured by dissecting the unique mouse. The use of small animal PET offers the possibility to keep the mouse alive, not only for one measurement but for several different times. In this way the single mouse will act as its own control and the interanimal variation is removed [4]. This thesis will focus on the imaging part of immuno-PET with development of a specific immuno-PET nuclide for prostate cancer (PCa). The strategy is to label monoclonal antibodies (mAbs) designed for the predominated proteins present in prostate, prostate-specific antigen (PSA) and human kallikrein 2 (hK2). A moderate increase of the PSA-level in blood might be an indication of prostate cancer (PCa), as well as a moderate increase of hK2-level, even though the latter is not clinical established as a diagnostic tool [5].

1.1 Purpose

The aim of this thesis is to produce and separate the radionuclide zirconium- 89 (^{89}Zr), for labelling of monoclonal antibodies (mAbs) If the mAbs are well-designed for the proteins combined with a successful labelling of ^{89}Zr, positron emission tomography (PET) might be an imaging modality to diagnose PCa. This work will also consist of phantom studies in a micro-PET to perform quantitative measurements of ^{89}Zr.

Below a purpose scheme is depicted, indicating that this work starts from scratch in Lund and shows roughly the necessary steps to the final goal – clinical studies.

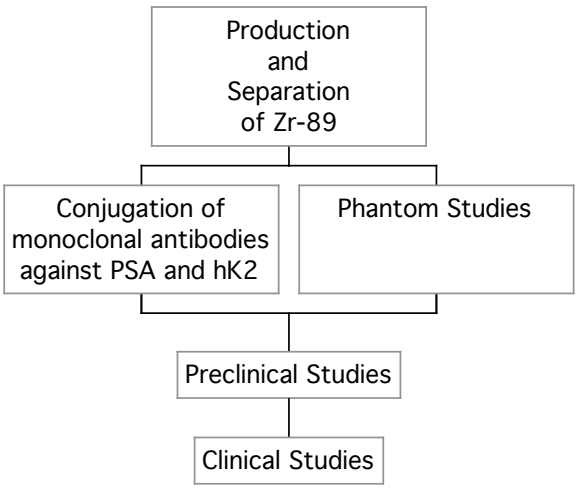

2 Background

2.1 Prostate cancer

In 2005, 9 881 men were diagnosed with PCa in Sweden which is 36% of all diagnosed cancer types among men. This makes PCa the most common cancer disease for men [6]. PCa is a disease of the elderly; most cases (> 66%) are diagnosed at an age of 70 or more, and it is rare that men below 50 years are diagnosed with PCa [5, 7]. The progression of tumour growth is normally a slow process, and most men diagnosed with PCa succumb due to other diseases or causes. On the other hand, some cases are subject of a more aggressive form, which starts quickly to give metastasis. It is hard to determine if the cancer has metastasised or will give metastases. An early diagnose of PCa, i.e. before it has begun to spread, is the only way to an effective treatment when curation is intended. Today, PCa is established by performing biopsies. In order to establish if the malignancy has metastasized to surrounding organs, a microscopic inspection of surgically removed pelvic lymph-nodes is needed. The high incidence of prostate cancer requires an easy and accurate tool to diagnose if the malignancy is of an aggressive form at an early stage, since an early diagnose enhances the chances to overcome the disease [5, 7].

2.2 Prostate specific antigen and human kallikrein 2

PSA is an enzyme that was originally isolated from seminal plasma but later even found in prostate tissue [5]. The protein originates mostly from columnar epithelial cells of the prostate gland, and is secreted into the glandular lumen. PSA is involved in the propagation process even though the details of physiological function are not fully understood. Normally, about 1 ppm of PSA in seminal plasma escapes into the blood-circulation, a leakage that is usually prevented by the cell wall in the basal layer [5, 8]**.** In blood, PSA has crossed the basal membrane, passed through the connective tissue (stromal layer) and finally crossed the capillary wall. A malignant growth is found to disorder the architecture of this cell structure in the sense of loss between epithelial cells and the basal membrane, which is thought to cause the increase of leakage of PSA into the bloodstream [9].

Most of the PSA in blood occurs in a bound state to certain enzyme inhibitors. About 65-95 % is complexed with α1-antichymotrypsin (ACT), which is the predominant enzyme inhibitor. The PSA not complexed with enzyme inhibitors assigns to free PSA that is a mixture of several PSA forms of which most are in an inactive state.

Increasing age conveys higher concentration of PSA in blood, which is mainly due to benign growth of the prostate resulting in an increased amount of epithelial cells, which implies more leakage of PSA to the blood-circulation [5].

The measurement of PSA (free PSA and PSA complexed to ACT) in blood is used today as an indicator for PCa and for treated PCa-patients. Very high levels of PSA in blood characterize advanced stages of PCa, while moderate levels might be an indication of early stage PCa as well as benign prostate hyperplasia or an inflammatory process. This means that the PSA-measurement alone cannot act as a predictor of PCa since it is not specific for tumour cells but for prostate cells [5, 10].

HK2 is another protein produced in the prostate, but not in the same extent as PSA (ca. 10-50% of the amount of PSA). Identical to PSA, the hK2 expression is androgen-regulated and released into seminal fluid [11]. HK2 and PSA display an extensive amino acid sequence identity (80%). Despite this, hK2 is believed to have a slightly different physiological role compared to PSA. HK2 may serve as a direct or indirect activator of proPSA [5]. hK2 is found to add important information to PSA for the diagnose of prostate cancer [12]. Immunohistochemical research in respect of hK2 has shown that hK2 is expressed in relation to the level of differentiation. This means that hK2 is expressed in a higher yield in tissue of low differentiation, such as tissue subjected to prostate cancer, and in a lower yield in tissue of high differentiation, such as tissue subjected to BPH. This is in contrast to PSA, where the PSA levels are found to be lower in PCa compared to BHP. Thus, a high ratio of hK2 to free PSA in serum is characteristic of aggressive PCa [11]. According to Darson *et al.*, hK2 is tumour associated since it is expressed in higher amounts in lymph node metastases [13].

Thus, visualization of PSA and hK2 could be a strategy to improve diagnostic accuracy in several senses. It could maybe replace biopsy or be used to detect lymph node metastasis, or it could be used to monitor the effect of radiotherapy or conclude whether a PSA production post surgery derives from non-removed glandular tissue or metastasis. Newly developed monoclonal antibodies against these two proteins opens up a possibility to combine them for diagnostic imaging and should be well suited for immuno-PET with the positron emitter ^{89}Zr.

2.3 Positron Emission Tomography

In the beginning of the 1950s the idea of using coincidence technique to image positron emitting radionuclides was proposed by Wren *et al.* With this idea they had realized the advantage of using coincidence technology between detectors. With this technology they wanted to study ^{64}Cu in brain tumours using opposing sodium iodine detectors. The Anger camera was launged on the market in 1954 and was quickly applied for positron emitters. Na(I) detectors with coincidence measurements were used in clinical investigations during the 1960s. In the beginning of the 1970s a very important progression in this field was done through the introduction of the tomography principle. The positron emission tomography (PET) technique is thus the outcome of two Nobel prize awards, the tracer principle (de Hevesy in 1943) and the tomographic principle (Houndsfield and Cormack in 1979) [14].

Since PET images generate physiological and functional information to the observer and the anatomic structures are sometimes hardly distinguished, PET is nowadays often combined with computed tomography (CT) to yield the anatomical information.

2.3.1 Basic Principle

Positron Emission Tomography is based on the coincidence detection principle of the two annihilation photons emitted after positron decay. A radioactive isotope, with an excess of protons, may disintegrate through positron decay. A proton in the nucleus is converted into a neutron, and at the very same moment a positron (β^+) and a neutrino (ν) is emitted. The positron has the same mass as an electron but the opposite electric charge, i.e. it is the antiparticle of an electron. In case of ^{89}Zr positron decay would look like:

$$^{89}Zr \rightarrow {}^{89}Y + \beta^{+} + \nu$$

The neutrino is always ejected simultaneously with the positron but is not detected. The energy released in the decay is divided between the positron and neutrino (and the residual energy of the daughter), which means that the positron energy is not monoenergetic but emits in a range of energies. For radionuclides used in PET the range of the positron in tissue is in the order of 1-10 mm [15].

Finally, when the positron reaches thermal energy, it interacts with an electron and form an unstable formation - positronium. Positronium eventually decays by emitting two anti-parallel annihilation photons corresponding to the rest masses of the electron and positron respectively, i.e. 511 keV each [16].

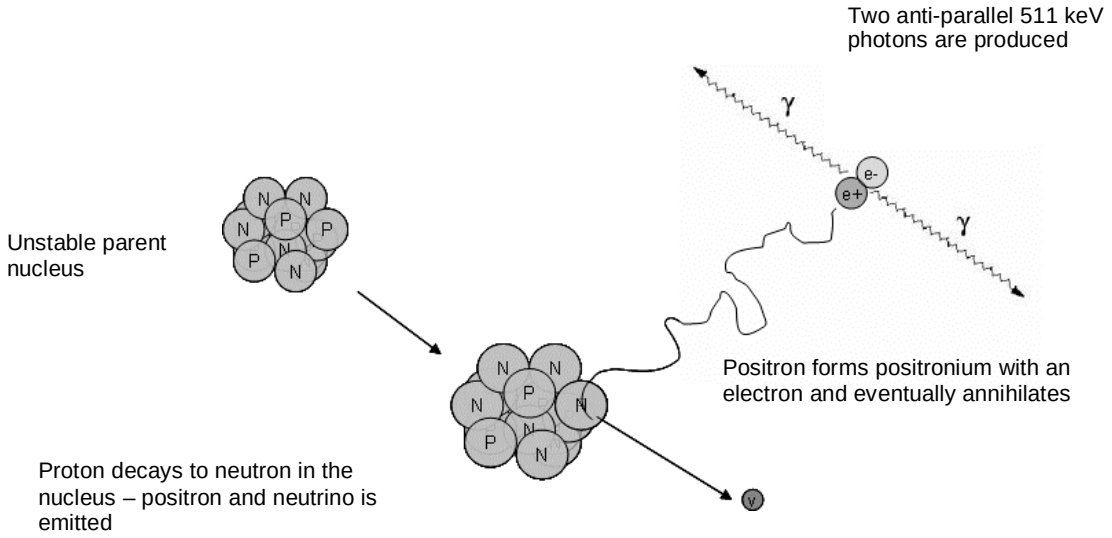

Figure 1. Basic principle of positron decay and the following annihilation. Due to inelastic collisions between the positron and atomic electrons, the positron can change its direction substantially from one collision to another.

The PET camera consists of a ring of detectors placed around the object to examine. If these two annihilation photons are registered in a very short period of time (~5-15 ns) the algorithms assume that anywhere along this line an event has happened, which refers to line of response (LOR). By calculating all LORs the place where the annihilation occurred can be reconstructed. This is basically the principle of coincidence systems. Notice that this location is not referred to the location where the positron decay took place, but to line along which the decay occurred [17].

2.3.2 Image degradation

The ideal situation for a coincidence measurement is an unscattered coincidence, i.e. a *true event*. Unfortunately this is not the case in most annihilation events. This *scattered coincidence* leads to a false LOR, which degrades the spatial resolution. Other scattered coincidences which degrade spatial resolution are *random coincidence* and *spurious true coincidence* [14, 17]. These events are illustrated in Figure 2.

Besides mechanical limitations (e.g. ring diameter, crystal size etc.) of the detector system, certain detector independent limitations are always present in PET. Positron range and photon non-colinearity are fundamental limitations in the physical nature of the positron decay. The former is characteristic for each positron emitter whereas the latter is independent of ditto. According to Verel *et al.* the resolution loss due to positron range from ^{18}F and ^{89}Zr is 0.7 mm and 1 mm respectively [17]. Non-colinearity describes the phenomenon that photons should intuitively be emitted anti-parallel to each other, but since the momentum must be preserved an angular uncertainty of ±0.5° is always present [14]. This will result in a false LOR. With a smaller ring diameter the spatial resolution loss due to e.g. non-colinearity is counteracted. Non-colinearity contributes about 1.5-2.0 mm in resolution loss for a whole body scanner (diameter 70-90 cm), and for head scanners (diameter 40-55 cm) this resolution degradation is reduced to about 1 mm. A further decrease of the detector ring decreases the contribution to spatial resolution loss of non-colinearity to about 0.2-0.6 mm for small animal scanners (diameter 10-25 cm) [18].

All together, the spatial resolution is determined of a number of factors, which can be summarized in the following equation:

$$FWHM = 1.2\left[\left(\frac{d}{2}\right)^2 + b^2 + \left(0.0022D\right)^2 + r^2\right]^{1/2}$$

where *d* is the crystal size, which is the limiting factor in most clinical scanners. *b* is called the block factor and is a mechanical and electronic limitation representing a systematic inaccuracy of detector positioning, and is a minor contributing factor. *D* is the diameter of the detector ring. *r* displays the contribution from the effective source size, namely the positron range in the subject. The factor 1.2 is the overall spatial resolution degradation from the reconstruction (filtered backprojection (FBP) and ramp filter) [18].

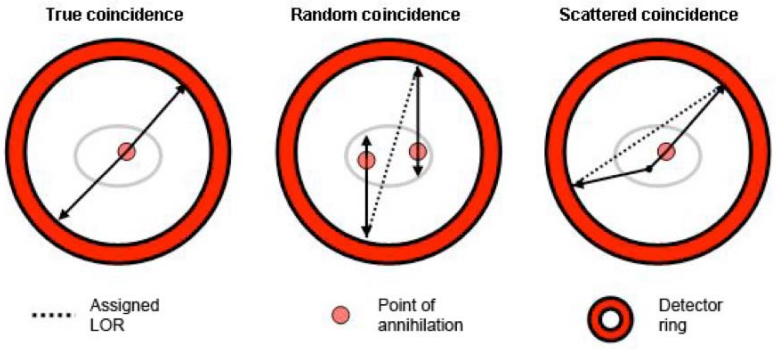

Figure 2. Different kind of coincidence events registered in a PET scanner. (a) *True events*, which are the registration of unscattered annihilation photons. (b) *Random coincidence*, i.e. two photons from different origins registered within the time window. (c) *Scattered coincidence*, where one of the photons are scattered. The Compton scattered photon still have the energy to trigger the energy window. *Spurious scatter* (not illustrated), i.e. the coincidence between a gamma photon and an annihilation photon. This problem is more pronounced in "dirty" positron emitters like ^{124}I.

2.3.3 Animal-PET

The difference in physical size between a human (~70 kg) and a laboratory rat (~300 g) or a mouse (~30 g) is a major challenge for the high-resolution system. To obtain the same image quality and to transfer the same biological question at issues from a human to an animal, same proportions between the physical volume of the object and the spatial resolution of the system must be required. In mouse models, very small structures of 1 mm or less (<1 µl in volume) are to be visualised and accurately measured to determine the accumulation of a certain radiopharmaceutical in different tissues. This is to compare to whole body studies of humans, where a typical spatial resolution lies in the order of ~10 mm (~1 ml in volume). To image structures in the brain and organs a resolution of at least 5-10 mm FWHM is sufficient, while in rat these structures are 10 times smaller (0.5-1.0 mm would be required), and further a factor of two would be required in mice. For clinical scanners the typical resolution is about 6-8 mm, while brain scanners can offer 2.5-3 mm. Animal scanners can provide a resolution better then 2.5 mm (best 1-1.5 mm) [18].

Whole-body human PET scanners have a sensitivity in the order of 0.3-0.6% in 2D acquisition mode and 2-4% in 3D. To conserve the same proportions from a human PET to a small animal camera, the requirement would be a sensitivity increase of a factor 1000. This is for the moment not possible, and the theoretical increase one can hope for is a factor ~300 in 2D mode and ~30 in 3D mode [19].

Besides the advantage in image quality, certain other practical advantages are provided by a dedicated animal PET system. The PET scanner can be sited in or at least very close to the animal laboratory and the housing facilities of the animals. This makes a clear distinction between the human clinic and the animal laboratory, something that might be preferred for the personnel and sometimes even mandatory by regulation authorities [20].

2.4 General demands on immuno-radionuclides

Despite the intrinsic limitations of the imaging system, certain requirements of the radionuclides and the radiolabelling work must be fulfilled to achieve satisfying results considering sensitivity, spatial resolution, quantification, and specificity. These are demonstrated below:

2.4.1 Physical half-life

In general, intact antibodies need 2-3 days to penetrate a solid tumour [21], after which an optimal tumour-to-nontumour ratio has been achieved. This requires a radionuclide with corresponding physical half-life [22-24]. Although a half-life in order of days is preferable according to the transportation of mAbs, this might be a drawback when considering radiation exposure to the patient. The increase of effective half-life means a higher absorbed dose to the considered tissue.

A rule of thumb in PET says that an examination should be done within 3 half-lives of the radionuclide, which in case of ^{89}Zr (T1/2=78.4 h) means that an investigation time window is available for almost 10 days [23].

2.4.2 Decay characteristics

Besides the requirement of being an abundant positron-emitting isotope of short range, the lack of no prompt γ-energies in the vicinity of the annihilation energy 511 keV is

desirable. These γ-energies might affect the accuracy of quantification while the positron range has influence on the resolution, especially in high-resolution PET where relatively small regions are of interest [24, 25].

2.4.3 Production

The production, through an irradiation of a target, with the aid of an *in situ* cyclotron is the choice to prefer. Further, the method of separation from the target must be simple and result in very high purity to not disturb the labelling of antibodies. This whole chain should be reproducible and to a low cost [24]. The relative long half-life of ^{89}Zr, enables a remote production in the absence of a cyclotron [26].

2.4.4 Labelling method

The fate of the radiolabel lies in the choice of the labelling method. The labelling method is of course dependent on the chemical nature of the radionuclide. E.g. ^{124}I is a halogen which usually attaches to the amino acid tyrosine, while ^{89}Zr which is a metal have found the most preferable labelling method with the aid of a chelating agent [23]. Differences in tissue accumulation between radiohalogens and radiometals have been observed [22]. This will be discussed later on in this thesis.

2.5 Zirconium

Zirconium is a metallic element in the group 4 (titanium family) with atomic number 40 [27]. In the mid-80s the isotope ^{89}Zr was found to be well suited in the field of immuno-PET by O´Brien and Link [28, 29]. Decay characteristics are illustrated in Figure 3. ^{89}Zr disintegrates through positron decay (22.7%) and through electron capture (73.3%) with a half-life of 78.4 h. The positron is emitted with maximum positron energy of 897 keV. In almost 100% of the decays the γ-energy 909 keV is present. The half-life 78.4 h and the sufficient high abundance of positrons makes this radionuclide well suited for antibody labelling with PET.

The first production of ^{89}Zr was done in 1951 by Shure and Deutsch at M.I.T. via (d,2n) reaction on Y_2O_3 [30]. A more preferable production is via a (p,n) reaction on a foil of ^{89}Y as target material. The natural abundance of 100% makes it ideal [31]. In view of the fact that production of ^{89}Zr is done via (p,n) (or (d,2n)) reaction enables the use of a cyclotron available to all PET-sites, or at least in the vicinity of one. Figure 4 shows the cross sections for the reactions ^{89}Y(p,n)^{89}Zr, ^{89}Y(p,2n)^{88}Zr and ^{89}Y(p,n)^{88}Y as a function of proton energy. As can be understood from Figure 4 the bombardment step involves the production of other metallic nuclides when the reactions diverges from ^{89}Y(p,n)^{89}Zr. Despite this, other radionuclides (^{48}V, ^{56}Co, and ^{156}Tb) are produced due to impurities of titanium, iron and gadolinium in the ^{89}Y-foil. These unwanted impurities must be separated from ^{89}Zr as they might compete in the labelling step with the antibodies [32]. The separating method that has yielded the highest purification is through a hydroxamate column, an anion-exchange column using hydroxamic function [24].

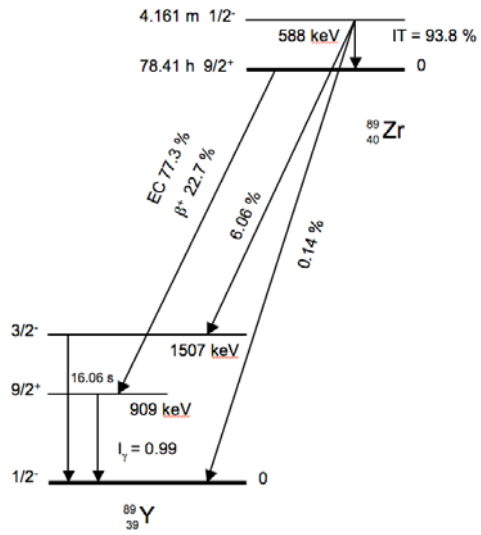

Figure 3. Decay scheme of ^{89}Zr including its metastable state. Data from Table of isotopes [33].

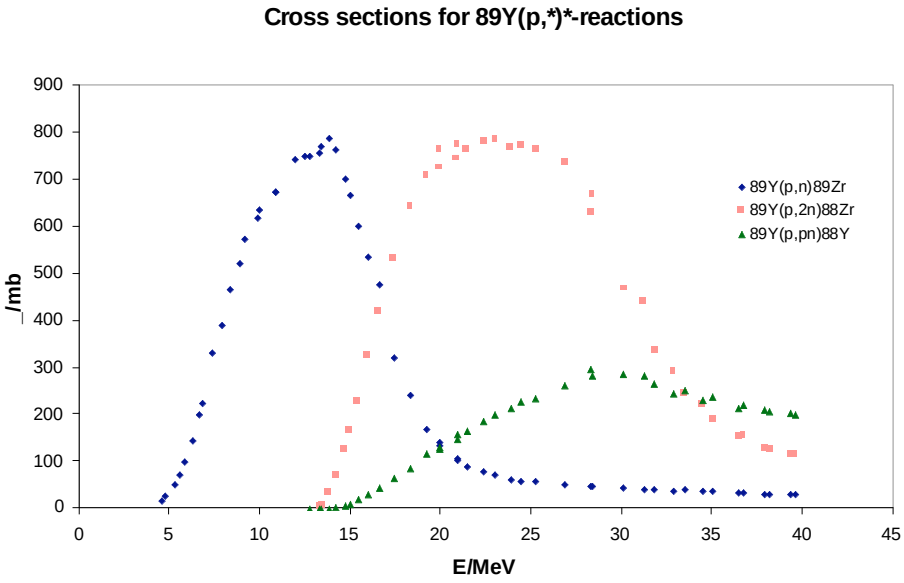

Figure 4. Cross sections for the reactions ^{89}Y(p,n)^{89}Zr, ^{89}Y(p,2n)^{88}Zr and ^{89}Y(p,n)^{88}Y. The optimal proton energy for ^{89}Zr-production and minimal production of ^{88}Zr and ^{88}Y is around 13 MeV. Data from [34].

2.5.1 ^{89}Zr vs. ^{124}I

As stated above, a predominant requirement of a radionuclide to be suitable for immuno-PET is its half-life. Two similar radionuclides are ^{89}Zr and ^{124}I whose decay characteristics are found in Table 1 and compared to ^{18}F and ^{64}Cu.

Table 1. Decay characteristics of four positron emitters. ^{18}F is present due to its common use in PET and its optimal characteristics in yield of positron decay and positron energy. ^{64}Cu is in included since it is a promising candidate in PET and RIT as well. Data from [17].

Positron emitter	Production	Half-life (h)	Main β^+-energies* (keV)**	(%)	Main γ-energies* (keV)	(%)	Intrinsic spatial resolution loss (mm)
^{18}F	^{18}O(p,n)	1.83	634	100.0	-		0.7
^{64}Cu	^{64}Ni(d,2n) ^{64}Ni(p,n)	12.07	653	17.09	-		0.7
^{89}Zr	^{89}Y(p,n)	78.4	897	22.7	909	99.9	1.0
^{124}I***	^{124}Te(p,n)	100.3	1535	11.2	603	62.9	2.3
	^{124}Te(d,2n)		2138	11.2	723	10.1	
	^{125}Te(p,2n)				1691	10.6	

*Energies <5% are excluded
**Maximum positron energy
***Positron emitter with >50 γ-energies

The much higher energies of the positrons emitted from ^{124}I is major drawback regarding intrinsic spatial resolution loss [17]. In addition, ^{124}I is a positron emitter with more than 50 γ-energies, and some of the energies are in the vicinity of 511 keV.

While the target material of ^{89}Zr is ideal in that sense of its 100% natural abundance, the target material for ^{124}I requires enrichment. This enrichment is for the moment very expensive, which means that care must be taken when handling the target in the everyday clinic [24]. The following distillation process of ^{124}I involves usage of gaseous radioactivity and due to iodine's volatile nature this implies additional care when considering radiation protection.

As prior mentioned, differences in the attachment to the antibody have been observed [23]. ^{124}I, who bonds directly to the antibody through tyrosine, becomes a subject of lysosomal degradation of the immunoconjugate resulting in the loss of iodotyrosine [21, 26]. The iodine then leaves the cell and enters the blood-circulation and accumulates in the thyroid or eliminates by the kidneys [21]. In case of radiometals (which utilizes the much stronger binding of chelates) this lysosmal degradation leads to accumulation in the cells instead of loss [26]. It is yet still very important that one uses a stable labelling to antibodies; otherwise the free radiometal will accumulate in marrow or bone, which might become a radiation hazard and generate bad images as wel[1, 22].

2.6 Production, separation and conjugation of ^{89}Zr

2.6.1 Production and Separation Chemistry

The production of ^{89}Zr starts at the cyclotron with the bombardment of protons on a 100% natural abundant ^{89}Y foil. Besides the ^{89}Y(p,n)^{89}Zr reaction, the production involves activation of impurities in the foil, which must be efficiently removed to not disturb the conjugation.

Some methods in the radiochemical separation of ^{89}Zr-isotope have been reported in the literature. This includes anion-exchange chromatography done by Dejesus and

Nickles [28] and anion-exchange column (Dowex) presented by Zweit *et al.* [32]. In the mid 60's it was found that the hydroxamic function had high specific affinity for Zr, even at high acid concentrations (> 1M HCl). So, at concentrations higher than 1M HCl, Zr is able to form complexes with hydroxamtes, whereas impurities like Fe, Al and Y are not. With this in mind one can use this observable fact to separate Zr through eluting the impurities with HCl. In this moment Zr is complexed in the resin and must be transchelated from the hydroxamate column in a solution appropriate for the labelling of mAbs. It was found by Meijs *et al.* [32, 35] that the most convenient solution was ≥ 0.5M oxalic acid. Verel *et al*. [24] have separated ^{89}Zr in oxalic acid with an overall yield of 97.0% ± 3.3% and a purity of more than 99.99%.

2.6.2 Conjugation chemistry

For reasons of *in vivo* use, a stable bond between the radiometal and the antibody is of crucial importance. If not, the accumulation of the radiometal is not representative for the biodistribution of the antibody in the patient.

When labelling antibodies with radiometals, one often uses bifunctional chelates, where bifunctional refers to that the complex should bind to the antibody as well as the radiometal. A chelating agent uses more than one atom that shares their electrons to the acceptoratom, i.e. the radiometal, through covalent bonding. Bifunctional chelates are frequently used in conventional ^{99m}Tc-chemistry, e.g. ^{99m}Tc-DTPA-albumin in lung scintigraphy [36]. For the binding of ^{89}Zr the bifunctional chelate desferal (Df) is ideal because of the stable bond between ^{89}Zr and the three hydroxamate groups in this complex [24]. An illustration of desferal is depicted in Figure 5. Df is the methanesulfonate salt of desferrioxamine which is produced by microorganisms for the transport of iron. It was found that Zr forms the most stable metal-hydroxamates complexes known, even more stable than with Fe[1] [37].

The stability of the Zr-Df has been measured and compared to Zr-DTPA in plasma solutions. According to Meijs *et al.* [37] less than 0.2% of Zr was lost in human plasma after 24 h compared to DTPA where 20% was lost.

A general structure when concerning bifunctional chelates would look like:

targeting molecule – linker – chelate - radionuclide [36].

The targeting molecule is in the case of prostate cancer a monoclonal antibody designed for either PSA or hK2. The linker is a molecule that acts like a bridge between the chelate and the antibody, where the linker unit developed by Verel *et al.* and used in this thesis, uses an amide bond (a chemical compound based on the reaction of an ester and an amine). Df contains an amino group that makes this linker chemistry possible, i.e. the amino group is the conjugation site where the chelate is covalently attached to the antibody through the linker [36, 37]. The method by Verel *et al.* conjugates Df directly to the amino acid lysine of the mAbs. This is based on a modification of the Df (*N*-sucDf) where a reaction between an active 2,3,5,6-tetraflurophenol-chelate ester (TFP-chelate ester) and the functional groups of lysine takes place. The method gives optimal control of the conjugation and the ability to quantify the numbers of groups coupled to the mAbs.

The use of lysine moieties of the mAbs opens the possibility to label not only intact mAbs, but also fragments of the antibodies or even peptides as long as the lysine group

[1] Desferal is used for treatment of acute iron poisoning.

is included. Another important advantage of this method is that *N*-sucDf appears in a condition where it is possible to label mAbs with ^{89}Zr efficiently without removing oxalic acid [24]. This means that a time consuming and a complicated step is no longer necessary [32]. A third advantage is that the method is based on the postlabelling of mAbs which makes it possible to produce mAb-*N*-sucDf at a remote site, while the coupling of ^{89}Zr can be done easily at the user's site. Thus, there exists a possibility for kit production that simplifies the clinical routines [24, 36].

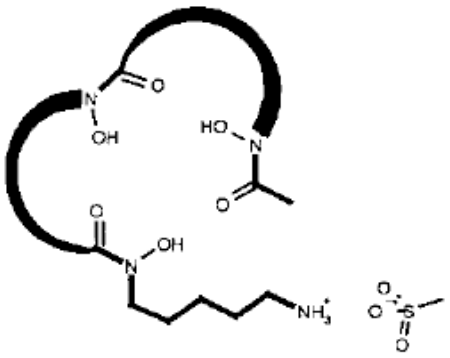

Figure 5. Simplified illustration of desferal (desferrioxamine B) with its three hydroxamate groups. A hydroxamate group consists of an amine (contain nitrogen as key atom) inserted into a carboxyl group, which in turn shares the same functional group. The "tail" in this figure represents the amine group where the antibody eventually is going to attach through the linker [24].

3 Materials and Methods

3.1 Production of Zr-isotopes

3.1.1 Irradiation in cyclotron

A target of 0.127 mm (0.005 in) thick foil of natural ^{89}Y (99.9%, Alfa Aesar) was bombarded with 16 MeV protons in a cyclotron (Scanditronix MC 16) for 1 h (16-17 μA). During irradiation the target holder, consisting of Al, was cooled with water.

Before purification, the target was dissolved in four successive portions of 0.5 mL 1M HCl (Sigma-Alrich). 0.1 mL of hydrogen peroxide (Sigma-Aldrich) was added to oxidize to Zr(IV), which is its usual oxidation state. This oxidation is important later on when Zr must be transchelated from the oxalic acid solution into the chelating agent Df. To receive a final concentration of 2M HCl 0.22 mL 12M HCl was added. This concentration is desirable to prevent hydrolysis of the Zr-chlorocomplex [32]. After addition of concentrated HCl, the solution was rested in 1 h.

3.1.2 Gamma spectroscopy

The production of ^{89}Zr must be verified. A radionuclide can be identified through its decay mode, emission energies and half-life. By gamma spectroscopy the present gamma energies in the sample can be analyzed, and therefore the presence of radioactive isotopes. To verify that ^{89}Zr actually has been produced and to reveal radionuclidic impurities co-produced in the irradiation of the ^{89}Y-foil, gamma spectroscopy with a HPGe-detector (GEM 100-s[2], relative efficiency: 123.1 % with Digidart (multi-channel analyser)) was done. Spectroscopic analysis where started quite early after end of bombardment (EOB) to verify the metastable state of ^{89m}Zr ($T_{½}$ = 4.2 min), as another proof of the ^{89}Zr-production. Data were collected during 600 s (real time) and at a relative large source-detector distance (~5.7 m) to minimize dead time. The collected data were then corrected for dead time.

The gamma spectroscopy was also done to quantify the amount of ^{89}Zr, which in turn was used in the calibration of a well-type ion chamber (Capintec CRC-5RB). By measuring the peak at 511 keV in ^{89}Zr, compare it to a known amount of ^{18}F in the same experimental set-up and in the same region of interest (ROI) as ^{89}Zr, quantification is possible. The ROI consisted of 21 channels (495-526 keV) around the peak of 511 keV. In this relative quantification the contribution from background activity was (within a very good approximation) assumed equal. However, the contribution from the 909 keV photons in ^{89}Zr was corrected by defining a check-ROI of 21 channels located 10 channels to the right at the ending of 511 keV ROI (542-573 keV). Within the check-ROI the background was subtracted to only quantify the photons originating from 909 keV. The counts from the check-ROI were then subtracted from the gross counts in the 511 keV peak of ^{89}Zr. The quantification measurement was performed when no ^{89m}Zr was left, i.e. after 1 h EOB. The ion chamber where in addition used to ensure that the half-life of the produced ^{89}Zr is correct (compared to the literature).

[2] Serial number: P41629A

3.1.3 Chemical separation of ^{89}Zr

^{89}Zr was purified from its radionuclidic impurities using a hydroxamate column. The column is based on a modified cation exchange where hydroxamate groups are introduced. To receive a high proportion of these added hydroxamate groups, the carboxylic acid groups of the cation exchange mass are esterfied in two steps using 2,3,5,6-tetraflurophenol (TFP, Acros Organics) solution (200 mg/mL in MeCN).

One g of cation exchange mass (Accel Plus CM, Waters) was suspended in 8 mL water for injection and well-mixed. 75 µL 3M HCl, 1 mL TFP-solution and 384 mg of 1-(3-Dimethylaminopropyl)-3-ethylcarbodiimide hydrochloride (EDC, Acros Organics) were added. The pH was measured to be within the acceptance interval 5.7-6.0. Then, the solution was mixed end over end in 1 h. In the second esterfication step 105 µL 3M HCl, 1 mL TFP-solution and 384 mg EDC was added after which pH again was measured to be within 5.7-6.0. To remove EDC and unreacted TFP, the solution was poured into a funnel with convenient filter and washed with 30 mL MeCN (Sigma-Aldrich). In the meantime the hydroxlaminehydrochloride solution, i.e. the solution containing the hydroxamate groups, was prepared. To a solution of 1 mL 1M NaOH (Sigma-Aldrich) and 2 ml MeOH, 690 mg of hydroxylamine hydrochloride (Sigma-Aldrich) was added. After 5 min another portion of 1 mL 1M NaOH was added and pH was expected to be within 5.3-5.4.

The washed esterfied cation exchange mass was then introduced to the hydroxylamine hydrochloride solution. Acceptance interval of pH is now 5.1-5.2. This solution was then mixed end over end over the night before it was washed in a funnel with filter as above. This time the columnmass was washed with 140 mL water for injection and 70 mL MeCN. The mass was then dried for 3 h in a vacuum chamber (Büchi Vacuum Pump V700, Vacuum Controller V-850) at room temperature. In the final batch, after the column mass had dried in room temperature during low pressure, the vacuum chamber was filled with argon to prevent humid air. After this “freeze drying” step, the column mass could be stored at room temperature up to 4 months without decreasing the labelling capacity of ^{89}Zr according to [24].

Before elution, the experimental setup was rinsed with 12M HCl and distilled H_2O. A 1.5 mL Extract Clean tube with belonging frit (Scantec Lab) was inserted into the arrangement. 100 mg of the hydroxamate column mass was suspended in 0.9% NaCl before it was packed into the Extract Clean tube. Thereafter the column was rinsed with 5 mL MeCN, 10 mL 0.9% NaCl and 2 mL 2M HCl. The ^{89}Zr-solution was then washed through the column initiated by a 5 mL Vacutainer (BD). To ensure that as much impurities as possible is absent in the resin, the column was washed with 6 mL 2M HCl and 6 mL of water for injection. Here after Zr was eluted in 5-7 portions of 0.5 mL 1M oxalic acid initiated by Vacutainers (BD). Each ^{89}Zr oxalate Vacutainer was then measured in an ionization chamber (Capintec CRC-5RB).

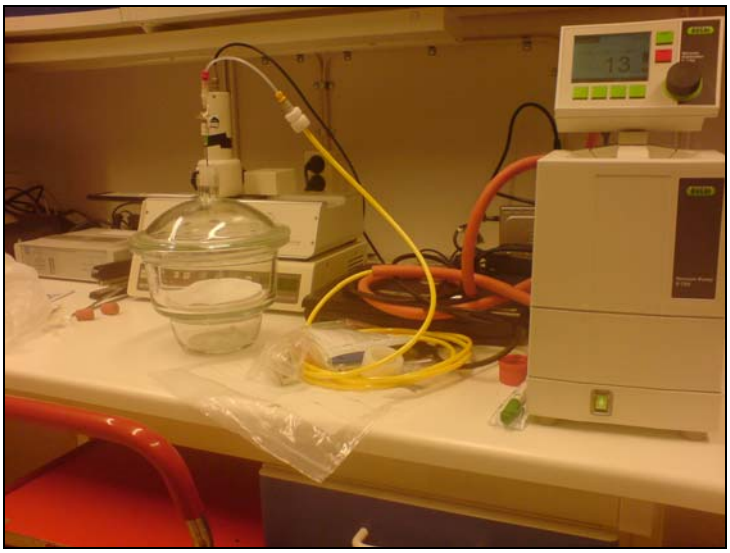

Figure 6. Equipment used for freeze-drying. The substance to be freeze-dried is placed in a chamber which is evacuated with a vacuum pump (Büchi Vacuum Pump V700 and Vacuum Controller V-850). Before placed in the vacuum chamber, the sample is stored in -20°C. In the final batch the chamber was filled with Ar to keep out humid air.

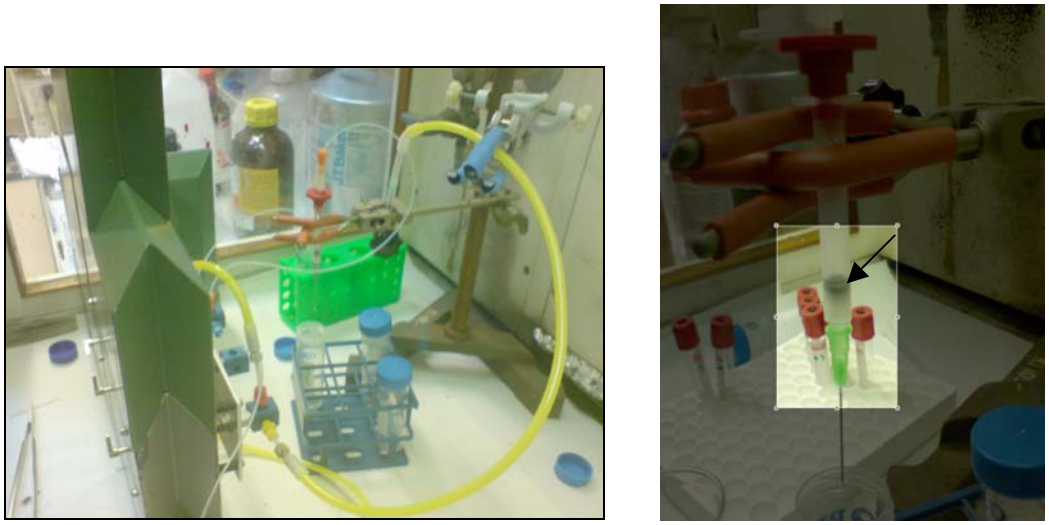

Figure 7. *Left.* Experimental set-up for purification of ^{89}Zr with the aid of a cation exchange column. *Right.* Zoom of the column. The gray layer is probably the result from oxidation of the Y-foil. The foil was delivered in Ar gas, but was kept under normal room conditions. This has affected the behaviour of the foil when it was dissolved. If this has had any impact of the ion exchange of Zr has not been investigated.

3.1.4 PIXE analysis

Samples of separated ^{89}Zr were sent for particle induced X-ray emission (PIXE) analysis to reveal stable impurities in ^{89}Zr oxalate. This analysis will then act as a quality control on the ion exchange mass.

PIXE is a sensitive technique for analysis of small amounts of elements. The method is based on the irradiation of protons, alphas or even heavy ions with a kinetic energy in

the order of MeV. The accelerated particles strike the sample to be analyzed, which might cause vacancies among inner electrons. These vacancies are quickly filled and result in characteristic X-ray emission. The K- and L-shell energies vary smoothly with different atomic numbers, and are therefore characteristic for each element. By observing the X-rays emitted, the presence of a certain sample can be deduced [38]. The Nuclear Microprobe at the Division of Nuclear Physics, Lund University, is a system including an accelerator of MeV-ions (1-4 MeV), probe forming magnetic lenses and a special irradiation chamber (with detectors), in which PIXE technique is possible [39]. The technique is very fast (10 s – 5 min) and sensitive. Very tiny amounts (10^{-12} g) of a sample can be analyzed. Up to 35 elements can be distinguished in a single sample [40].

One batch of irradiated ^{89}Y-foil was dedicated for PIXE analysis. After the foil was dissolved in the same way as mentioned above, five portions of ^{89}Zr was eluted in oxalic acid. Small amounts were successively pipetted on five plastic sample trays designed for PIXE analysis. Each sample was left to be evaporated in room temperature until next pipettation. This was repeated until the whole batch was evaporated.

Figure 8. Sample disc for PIXE analysis.

3.2 Conjugation of mAbs to ^{89}Zr

Premodification and conjugation of mAbs with ^{89}Zr is basically a six step process. (*Step 1*) The synthesis starts with carboxylation of the primary amine of Df creating *N*-succinyldesferrioxamine B (*N*-sucDf), which makes the conjugation possible (Figure 9). It starts with 2.5 g Df (Novartis) which was added to a solution of 8.5 g succinic anhydride (Aldrich) in 37.5 ml pyridine (Sigma-Aldrich). During 24 the solution was stirred in room temperature after which Df was completely dissolved. 300 ml of 0.30 M NaOH (Sigma-Aldrich) was then added during stirring to convert the surplus of succinic anhydride to succinic acid. After another 2 h of stirring the pH was lowered to 1.1 with 12 M HCl. The solution was placed in a refrigerator for 16 h after which the white product *N*-sucDf has precipitated. To remove the excess of unreacted succinic acid ice-cold 0.01 M HCl were added. After shaking, the solution was decanted. Ice-cold 0.01 M HCl were added again, shaked and decanted. This procedure was repeated a 3-5 times. After the final decantation 35 ml of ice-cold 0.01 M HCl were added to start the crystallization process. The product was slowly heated until boiling under stirring. At temperatures above 75°C the white product starts to dissolve. At boiling temperature (100°C) the product was completely dissolved, i.e. a totally clear solution was achieved. The solution was then slowly cooled off in room temperature for 4-5 hours before it was stored in the refrigerator over the night. About 16 h later the crystals had precipitated

and was filtered through a funnel with paper filter. The product was then put in the freezer for 5-7 of hours before it was dried in a vacuum chamber (same as Figure 6).

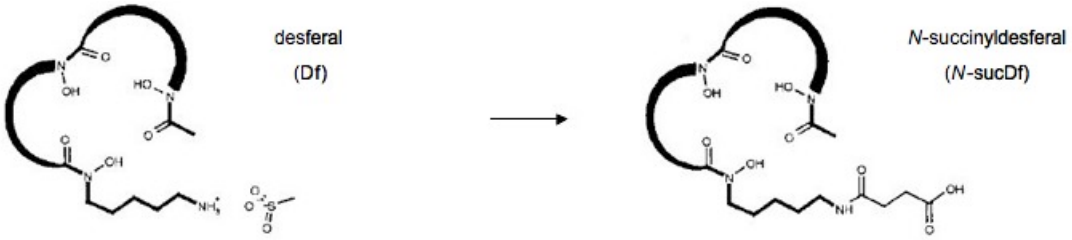

Figure 9. Illustration of the synthesis of *N*-sucDf. *Step 1* as described above is the convertation of the amine group in Df to a carboxyl acid group in *N*-sucDf. This makes the conjugation with the aid of an active TFP-ester possible. Reprinted with permission from the authors [24].

Step 2 is the temporal blockage of the hydroxamate groups of *N*-sucDf with Fe(III). The blockage with Fe(III) is a preparation before the next step described further down. In 60 µl 0.1 M Na_2CO_3 (Merck) and 3 ml 0.9 % NaCl, 9 mg of *N*-sucDf was dissolved. The pH was measured to be within 6.5-7.0. Otherwise pH was adjusted with more Na_2CO_3. 300 µl of $FeCl_3$-solution (8 mg/ml in 0.1 M HCl, Sigma-Aldrich) was added where after the solution rested for 10 min.

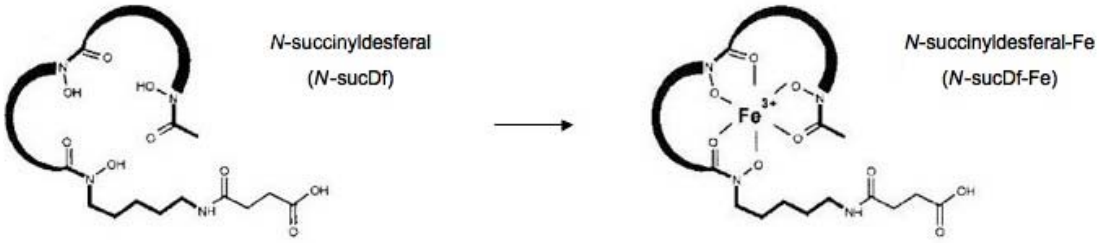

Figure 10. *Step 2*. Complexation of *N*-sucDf with Fe(III). The iron has occupied the three hydroxamate groups in *N*-sucDf. Reprinted with permission from the authors [24].

The third step (*Step 3*) is the synthesis for the esterfication of *N*-sucDf-Fe with TFP ester, the foundation of this method. To the solution from *Step 2*, 300 µl TFP-solution (200 mg/ml in MeCN) and 120 mg EDC were added. The pH was measured and adjusted with EDC to be within 5.8-6.0. To prevent reactions against Df with EDC the iron blockage was essential, which is the motivation of *Step 2*. EDC is a carbodiimide that acts as an activator of the introduced carboxylic groups towards an ester. The obvious thing to do would be blocking with ^{89}Zr, but it was found by Verel *et al.* that the synthesis would not yield the pleased amount of TFP-*N*-sucDf-^{89}Zr [24].

After pH was adjusted the solution was incubated in room temperature for 45 min. In the meantime a Sep-Pak C_{18} cartridge (Waters) was conditioned with 10 ml MeCN and 10 ml water for injection. After incubation, the cartridge was loaded with the incubated

solution where after it was rinsed with 60 µl water for injection. TFP-*N*-sucDf-Fe was finally eluted with 1.5 ml MeCN. The product was dispensed in 50µl/vial and then placed in a freezer (-80°C). TFP-*N*-sucDf-Fe could from here be stored for at least 8 weeks.

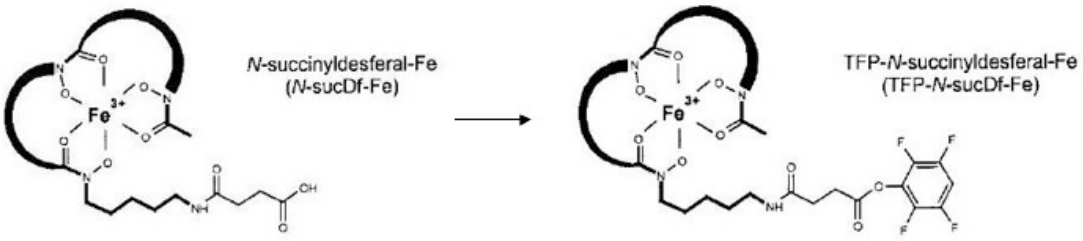

Figure 11. *Step 3*. The esterfication of *N*-sucDf-Fe. The introduction of TFP is the essential part in the premodification Df, which enables a stable bond between the cheater Df and mAb. Reprinted with permission from the authors [24].

A first attempt to conjugate mAbs to TFP-*N*-sucDf-Fe (*Step 4*) has been made. Even though we had access to mAbs designed for PSA, they were not used due to their high cost. Instead conjugation was tried with Rituximab[3] (Roche), a commercially available antibody. A protocol received from the staff at VU University, Amsterdam, was followed. Since this protocol in fact was based on the conjugation of Rituximab, it was well suited to follow this line.

To 500 µl Rituximab (5 mg), 470 µl NaCl 0.9% was added and gently swirled. The pH was measured to 6.57 and adjusted stepwise to 9.75 with 20 µl 0.1 M Na_2CO_3. Recommended range lies within pH = 9.5-9.7 that means the pH of the sample was a little bit high. To one vial (50 µl) of TFP-*N*-sucDf-Fe, 86 µl MeCN was added to achieve a solution of 3.3 nmol/µl MeCN. Then, 20 µl of this solution was added to the Rituximab solution and incubated for 30 min in room temperature during manual vortexing. As a quality control, 60 µl of this solution was reserved for HPLC analysis.

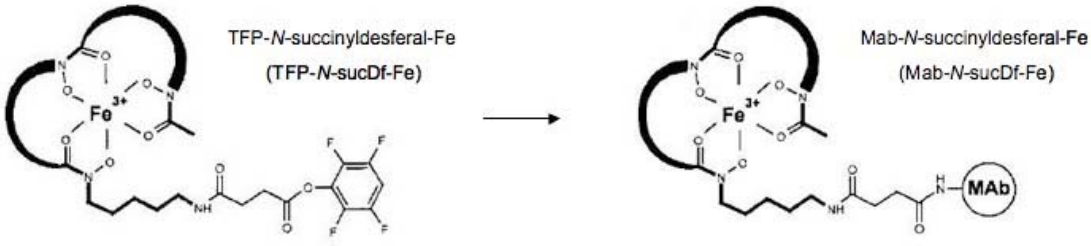

Figure 12. *Step 4* involves the conjugation of the antibody to the linker of Df. Reprinted with permission from the authors [24].

[3] Rituximab is used among others in treatment for non-Hodgkin's lymphoma and leukemia.

In *Step 5*, 2 times 25 µl 100mg/ml gentisic acid sodium salt hydrate (Sigma) was introduced to not risk a degeneration of the mAbs due to radiation. pH was measured to 6.8 and lowered to 4.50 with 30 µl 0.25M H_2SO_4 (Sigma-Aldrich) (acceptance range: 4.20-4.50). 50 µl 25 mg/ml of EDTA (ethylenediaminetetraacetic acid, Sigma-Aldrich) was added to take care of the unreacted Fe in the sample. The solution was then incubated at 35 °C during 30 min and carefully stirred. In the meantime a PD-10 column was rinsed four times with 4 ml 5 mg/ml gentisic acid. After incubation the Rituximab-*N*-sucDf-Fe was applied to the PD-10 column. 1.5 ml 5 mg/ml gentisic acid was pipetted into the column and the eluant was discarded. The next 2 ml 5 mg/ml gentisic acid applied to the column was collected. At this moment, unreacted EDTA, TFP, Fe and *N*-sucDf are supposed to be removed from the reaction mixture which should only contain Rituximab-*N*-sucDf.

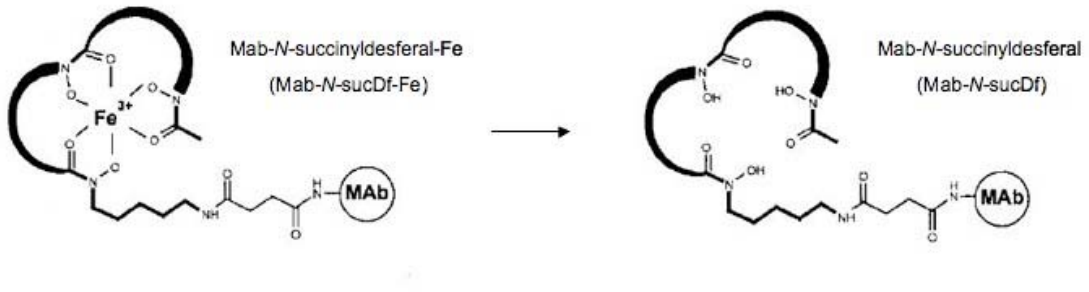

Figure 13. *Step 5*. The Fe that has been blocking the hydroxamate groups is in this step going to be removed through a PD10 column with 5 mg/ml gentisic acid as eluent. Reprinted with permission from the authors [24].

The final step remains (*Step 6*), i.e. the ^{89}Zr labelling. Unfortunately, just a low radioactivity concentration of ^{89}Zr was available which meant a low starting activity of 0.6 MBq (0.200 ml ^{89}Zr oxalate). 90 µl of 2M Na_2CO_3 was added and the mixture was gently swirled for 5 minutes. Verel *et al.* [24] found that it was possible to transchelate ^{89}Zr oxalate into Df efficiently within an optimal pH range of 7.2-7.4. This requires a strong buffer, where HEPES (Sigma) was found suitable. Therefore, 300 µl 0.5M HEPES was added, followed by 710 µl Rituximab-*N*-sucDf and additional 700 -sucDf and additional 700 µl 0.5M HEPES. The reaction mixture (2 ml) was incubated for 1 h.

Reaction mixture of 5 µl was pipetted on ITLC (0.02M citric acid as mobile phase) and cut into nine pieces. Each one was thereafter measured in a gamma counter (*1282 Compugamma CS, LKB Wallac*). During incubation a PD-10 column was washed four times with 5 mg/ml gentisic acid. The reaction mixture was added to the PD10 column and together with the first 1.5 ml 5 mg/ml gentisic acid, the eluents were discarded. 500 µl 5 mg/ml gentisic acid was added and collected in twelve fractions. If Rituximab-*N*-sucDf-^{89}Zr has been successfully produced, fraction 4-8 should contain the labelled antibodies.

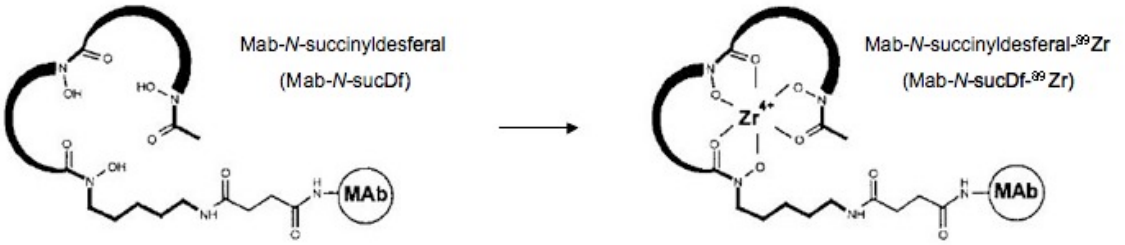

Figure 14. *Step 6.* After removal of Fe, ^{89}Zr is introduced. The ^{89}Zr oxalate is transchelated into mAb-*N*-sucDf during the presence of a strong buffer in a narrow pH range (7.2-7.4), namely HEPES. Unreacted HEPES should be removed in the PD10 column. Reprinted with permission from the authors to [24].

3.2.1 Quality control

Quality control when concerning nuclear pharmacy includes not only radionuclide identification done by HPGe-spectroscopy and determination of radionuclidic purity, but also the radiochemical identification. The radiochemical identity is in this thesis done by HPLC.

3.2.1.1 HPLC analysis

High-performance liquid chromatography (HPLC) is an analytical chemistry-based method to separate chemical compounds in a sample. Chromatography in general uses the fact that different compounds are transported differently in a stationary and a mobile phase. In HPLC, liquid is used as mobile phase while the stationary phase is often some kind of ion exchanger. The stationary phase is then packed in a column while the liquid is eluted through the column. The compounds, which are to be separated, are transported through the column. A compound that is not adsorbed in the stationary phase is eluted in the same pace as the liquid phase, while a compound that adsorbs will be delayed (retarded) in its transport through the column. Different compounds, which will interact differently with the column, will therefore be separated more or less. After the passage through the column a detector will register the presence of the separated compounds. The detector is often an ultraviolet (UV) spectrophotometer, while working with radiopharmaceuticals a radiation detector is necessary. For UV detector system the change of absorbed UV light is recorded and displayed as a chromatogram peak. When a radiation detector is used the concentration of radioactive components in the elute is analysed [36, 41].
The result is presented by a chromatogram which is a graph with the concentration of a certain compound as a function of the retention time, i.e. the time it takes to pass through the column [41]. The smaller the compounds, the longer retention times.

3.3 Phantom studies

A first attempt to perform phantom studies on a MicroPET Focus 120 was done at the Panum Institute, Copenhagen University. The properties of spatial resolution and sensitivity of ^{89}Zr compared to ^{18}F were measured. Phantom studies were continued in Lund at the GE 4096 *Plus*, which is a clinical whole body PET scanner.

3.3.1 MicroPET Focus 120

3.3.1.1 System description

MicroPET Focus 120 (Siemens Medical Solutions) at the Panum Institute is a ring-type PET scanner with high-resolution and high-sensitivity intended for small animal experiments. The detector array consists of 96 detector blocks (4 rings with 24 blocks in each ring). Each block consists of 12 × 12 (1.5 × 1.5 × 10 mm^3) lutetium oxyorthosilicate (LSO) crystals. Position-sensitive photomultiplier tubes are connected the LSO crystals through an 8 × 8 bundle of optical fibres. The diameter of the ring is 15 cm and the system has an axial FOV of 7.6 cm. PET data are acquired in list mode and can be reconstructed by various techniques [42]. Reconstruction techniques used in the measurements in this thesis were filtered backprojection (FBP) and 3D maximum posteriori (MAP).

3.3.1.2 Spatial Resolution

A spatial resolution phantom was constructed with plastic tubes with an inner diameter 0.254 mm (0.01 in) and an outer diameter of 1.5 cm. The thickest part was constructed to totally cover the axial FOV of the PET system and measures 9 cm, while the inner tube was made longer, so the activity could be homogenously distributed throughout the phantom. The volume of the phantom was 0.015 ml and filled with approximately 230 kBq ^{89}Zr and 410 kBq of ^{18}F. The phantom was placed in the central FOV (CFOV), 38 mm off-axis and 28 mm tangential, which is illustrated below (Figure 15). Data were collected during 10 min and reconstructed with FBP and MAP.

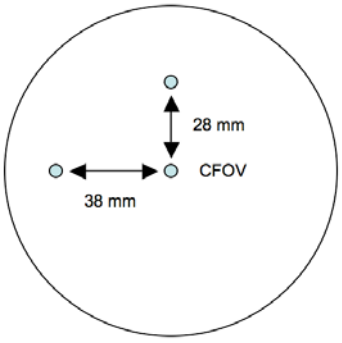

Figure 15. Locations of the phantom according to transaxial central FOV.

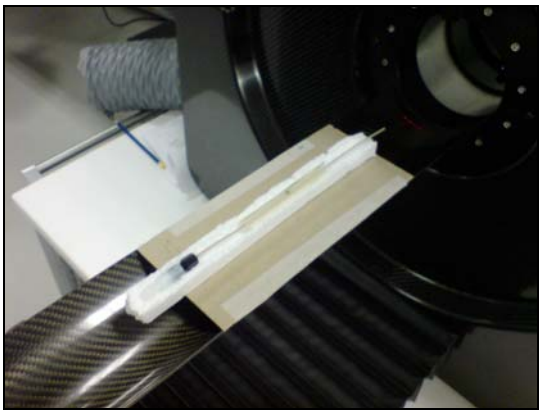

Figure 16. The spatial resolution phantom at the couch of the MicroPET Focus 120.

3.3.1.3 Sensitivity

The sensitivity phantoms consisted of syringes (110 × 30 mm) filled with 20 ml of 34 kBq/ml ^{89}Zr and 17 kBq/ml ^{18}F, respectively, and were placed in CFOV as depicted in Figure 17. Data were collected during 10 min and reconstructed with FBP.

3.3.2 GE 4096 *Plus*

3.3.2.1 System description

GE 4096 *Plus* is a whole body clinical PET scanner containing eight rings of 512 crystals each, which adds up to a total amount of 4096 crystals. The crystal consists of bismuth germanate (BGO) with dimensions 6 × 12 × 30 mm^3. Two dual photomultiplier tubes are connected to a matrix of 16 crystals. Crystal ring diameter measures 1010 mm and the eight rings give an axial FOV of 103 mm. Data are collected in 2D mode.

3.3.2.2 Sensitivity

Same type of syringes used in the MicroPET Focus 120 and depicted in Figure 17 were filled with 232 kBq/ml ^{89}Zr and 34 kBq/ml ^{18}F respectively. Data were collected during 10 min in the GE 4096 *Plus* scanner, with the phantom located in the CFOV. Corrections were made for attenuation and scatter.

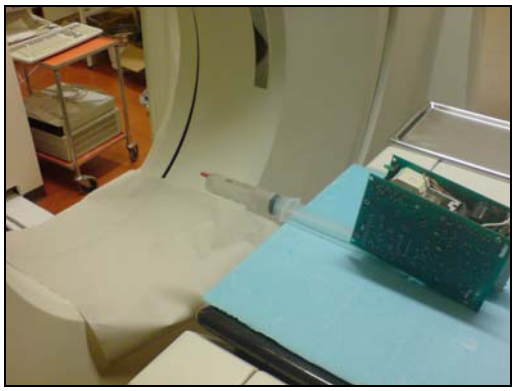

Figure 17. Set-up for sensitivity measurement in whole body PET scanner (GE 4096 *Plus*). The phantom was placed free in air to avoid attenuation from the bunk.

3.3.2.3 Scatter contribution

A comparison of scatter contribution between ^{18}F and ^{89}Zr was measured in GE 4096 *Plus* with the phantom in Figure 18. 35 MBq ^{18}F diluted in water filled the phantom and was measured for 30 min. Because of the lower activity (10 MBq) and lower positron abundance, the ^{89}Zr was measured for more than 4 h to achieve the same counting statistics as for ^{18}F. Data were iterative reconstructed and corrected for attenuation and scatter based on ^{18}F as well. A profile through the cold spot was thought to demonstrate the scatter fraction. The relative scatter fraction is measured by comparing the ratios of activity concentration in the hot part and in the cold insert for ^{18}F and ^{89}Zr respectively.

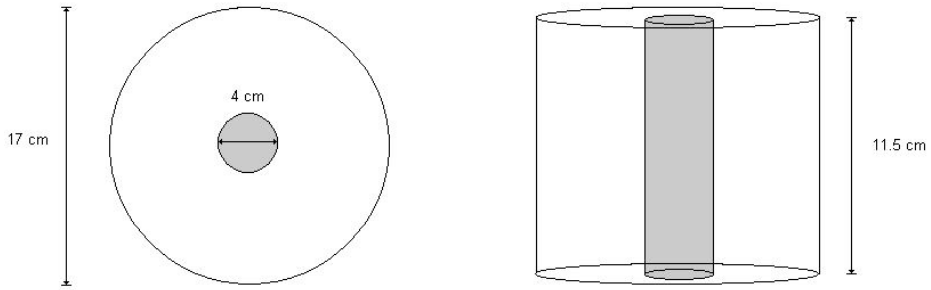

Figure 18. Dimensions of the scatter phantom with a Lucite cylinder inserted acting as a cold spot. The phantom was filled with radioactivity diluted in water.

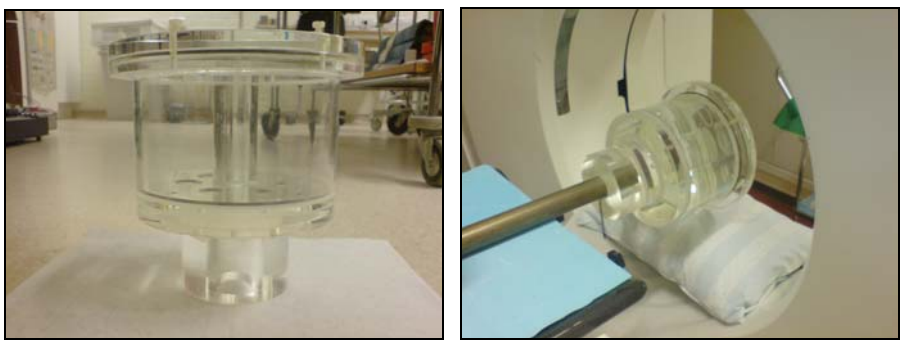

Figure 19. *Left* Lucite scatter phantom with inserted cylinder in centre. *Right* Positioning of scatter phantom in GE 4096 *Plus.*

4 Results

4.1 Production

Figure 20 below shows the spectra measured from the HPGe-detector 21, 35, 43 and 78 min EOB. Peaks not originating from background radiation are marked. From this spectroscopic analysis the production of ^{89}Zr could be verified with its characteristic energies as well as its metastable state. Notice how the amount of the metastable state of ^{89}Zr decreases as the time after EOB increases. Due to the short half-life of ^{89m}Zr ($T_{½}$ = 4 min), it has completely decayed after 1 h EOB. When the ^{89m}Zr has decayed it is convenient to do the relative quantification with a known radioactivity of ^{18}F.

The spectra also reveal the co-production of ^{88}Zr, which is in agreement with cross sections found in Figure 4. No quantification of ^{88}Zr has been carried out.

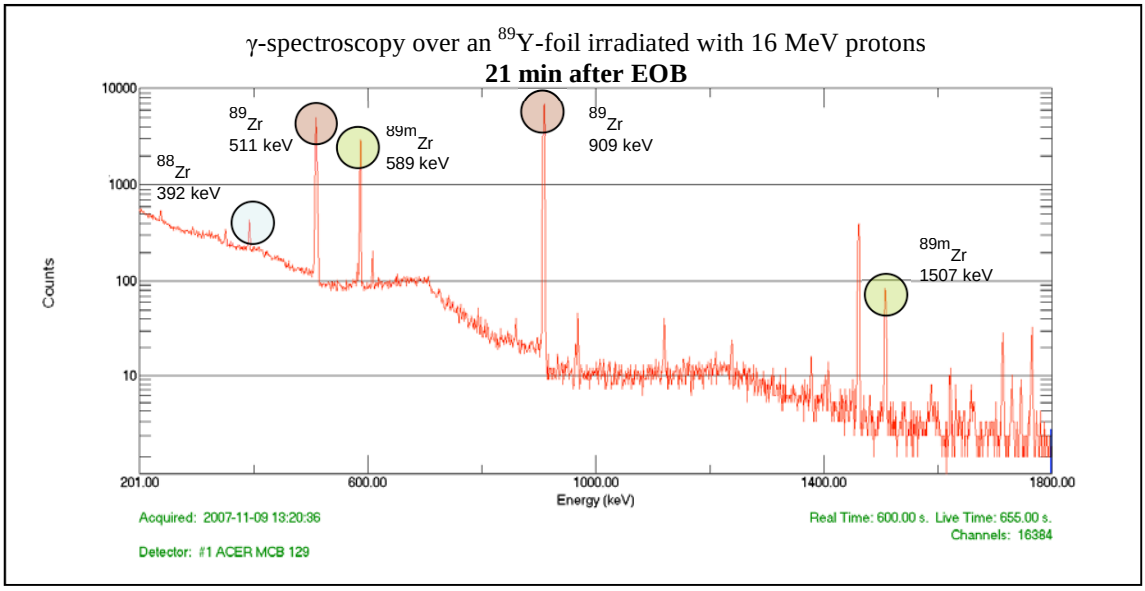

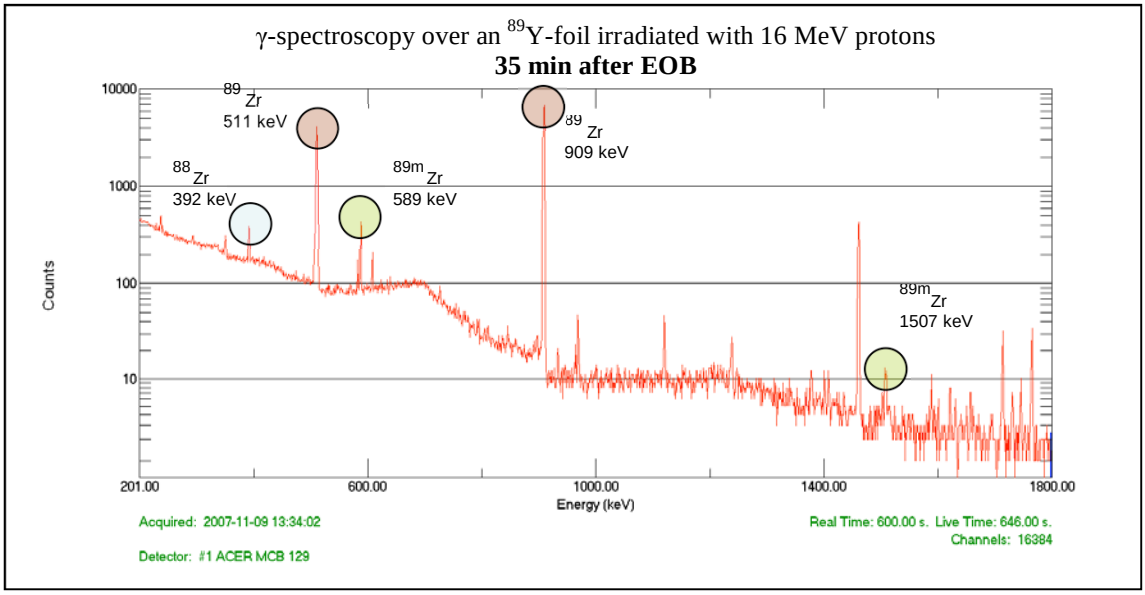

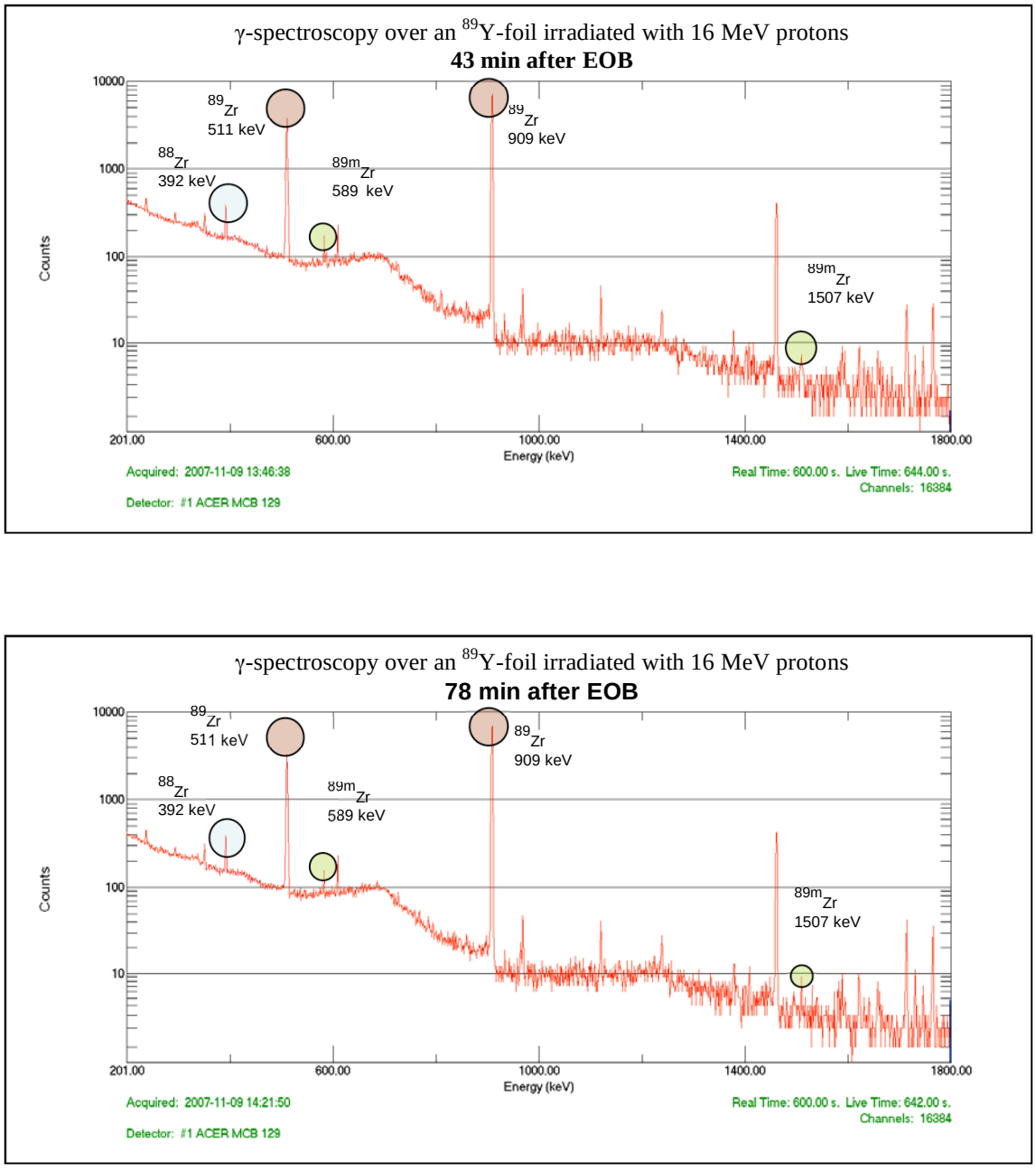

Figure 20. γ-spectroscopy acquired for 600 s (real time, dead time ~6.5-8.5 %) with HPGe-detector 21, 35, 43 and 78 min EOB. The characteristic gamma energy (909 keV) with nearly 100 % abundance from ^{89}Zr is clearly seen in these spectra, as well 511 keV originated from positron annihilation. The γ-spectroscopy was initiated quite fast after EOB to verify the metastable state of ^{89}Zr. ^{89m}Zr has a half-life of approximately 4 min (as depicted in Figure 3) and has characteristic energies of 589 keV and 1507 keV. As can be seen by these four spectra ^{89m}Zr has in principle decayed after an hour (observe the logarithmic scale). The presence of ^{88}Zr is also verified with its characteristic energy of 392 keV.

4.2 Separation

In Figure 21 the elution profiles of ^{89}Zr through a hydroxamate column are depicted as percentage of the initial radioactivity from the dissolved foil. In all, four separations were carried out. The radiochemical yield was a least 83 %.

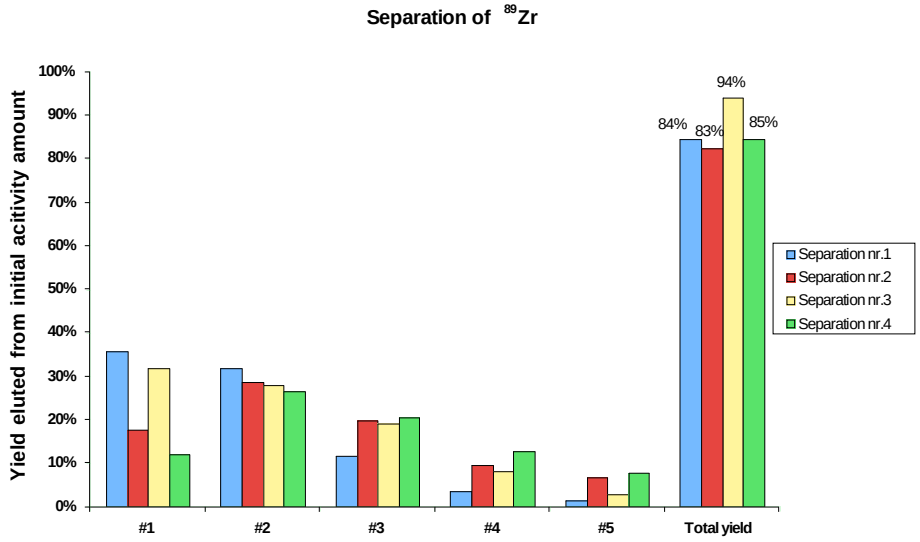

Figure 21. Elution of ^{89}Zr in oxalic acid from a hydroxamate column. Total yield refers to the five (#1-5) elutions added and compared to the initial amount of radioactivity (dissolved foil). In separation nr 3 additional two elutions were done since a significant amount of activity was found to be still in the column. These elutions increased the total yield with 3 %. The initial activities were 2.3, 5.9, 35.9 and 11.7 MBq respectively.

The half-life of ^{89}Zr was roughly estimated through an ion-chamber to ensure to be in accordance with the half-life found in the literature (78.41 h). Six measurements were done during almost six days. This measurement considered indirectly the stability of the ion-chamber as well.

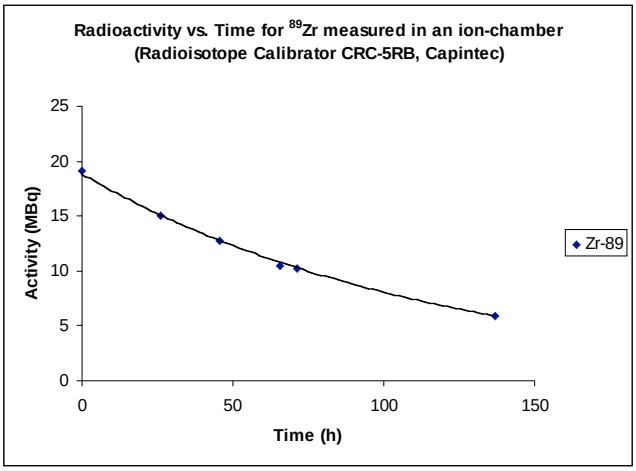

Figure 22. Radioactivity as a function of time. Data from one single continuous measurement. An exponential regression (R^2=0,9982) was done to verify the half-life of ^{89}Zr. Experimental half-life was calculated to 81.5 h compared to 78.4 h [33]in literature. This experimental result differs within 4 % compared to the literature.

4.3 Conjugation

The attempt of conjugation did not happen as expected this first time. Figures below are important to find out what went wrong. For the HPLC analysis, it was found that Rituximab had high absorbance at a wavelength of 215 nm. All figures below use this wavelength.

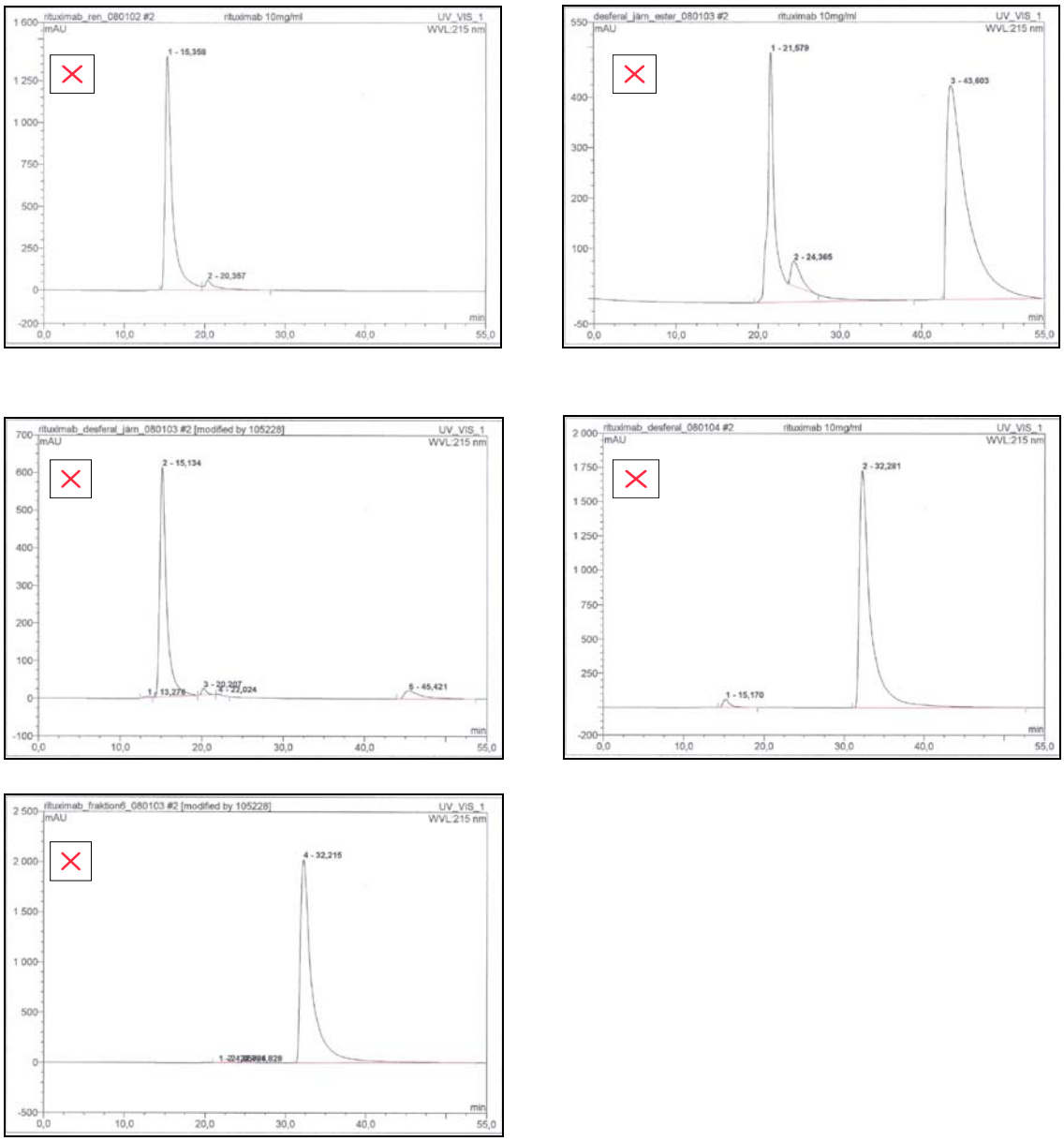

Figure 23. Results from HPLC analysis at 215 nm in the conjugation process. *(a)* Rituximab (10 mg/ml), *(b)* TFP-*N*-sucDf-Fe diluted in MeCN, *(c)* Rituximab-TFP-*N*-sucDf-Fe, *(d)* Rituximab-TFP-*N*-sucDf and *(e)* Rituximab-TFP-*N*-sucDf-^{89}Zr sample 6.

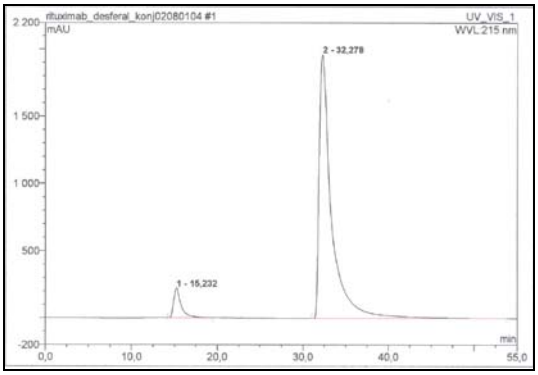

Figure 24. The complexation of Rituximab-TFP-*N*-sucDf (*Step 5)* was repeated due to the low yield of after PD-10 column in Figure 23.

In Figure 23 *(a)* Rituximab is identified at a retention time of 15 min while the peak at 20 min probably is fragmented Rituximab. A test of the esterfied Df filled with Fe, TFP-*N*-sucDf-Fe (refer to outcome of *Step 3*), diluted in MeCN was done. The intact compound is thought to be found at 24 min, while the peak at 21.5 min probably represents the unstable formation of this compound since it is not stable in room temperature. If a wavelength of 430 nm is used, the areas are reversed (not shown), which means that the quantification should at this stage not be taken too seriously. In other words, further investigations must be done if quantification is intended. These spectra will then in principle only show the presence of certain compounds. Unreacted MeCN is thought to cause the peak at retention time 43 min. In Figure 23 *(c)* the analysis of the conjugation of Rituximab to the Df complex (*Step 4*) is shown. The peak at 15 min indicating Rituximab is clearly seen, but with half of the area under the peak compared to the "clean" Rituximab in *(a)*. This is in accordance with the diluted concentration of Rituximab in *Step 4* (see Materials and Methods). *Step 5* concerns the removement of Fe as well as unreacted EDTA, TFP and *N*-sucDf. The peak at 15 min is approximately one tenth of that in *(c)*, which means practically no elution of complexed Rituximab from the PD-10 column – everything is probably stuck in the column! The large peak at 32 min is thought to be unreacted gentisic acid. Figure 23 *(e)* shows the analysis of sample 6 from the final step, i.e. the labelling of ^{89}Zr. Here is the complete failure shown – no peak at all at 15 min indicating no Rituximab. The eluted samples were measured in an ion chamber that indicated almost no radioactivity.

The conjugation until *Step 5* was repeated due to this failure. But since the lack of time and the unsufficient amount of ^{89}Zr, no labelling was carried out. The ending is shown in Figure 24 with a peak area about 35- 40 % of that in Figure 23 *(c)*. Thus, this elution was more successful but still over 60 % of the complexed Rituximab is lost in the PD-10 column.

4.4 Phantom studies

4.4.1 Spatial resolution

Spatial resolution measurement in a MicroPET Focus 120 with a line source located in CFOV, 28 mm transaxial and 38 mm radial. Two reconstructions methods were used, filtered backprojection (FBP) and maximum a posteriori (MAP). In Figure 25 a

reconstructed sagittal slice of the spatial resolution phantom filled with ^{89}Zr placed 38 mm off-axis is depicted. The radioactivity is injected in the bottom of this figure and is a bit inhomogenously distributed.

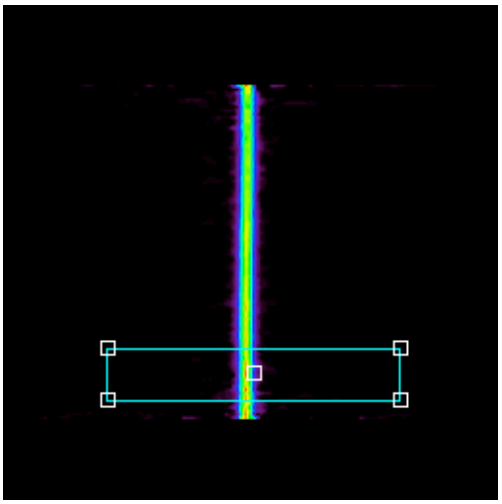

Figure 25. "Visualisation" of the resolution phantom containing ^{89}Zr. This picture represents a sagittal slice of 38 mm off-axis FBP reconstructed phantom. The rectangle is the ROI where the spatial resolution profile was measured. The lower side of the picture represents the part where the activity was injected, which is a bit hotter than the upper indicating a not perfect homogenous distribution of ^{89}Zr.

In the picture above a profile over the phantom was drawn in the hottest area, i.e. in the lower part of Figure 26. From this profile the spatial resolution (FWHM) was determined.

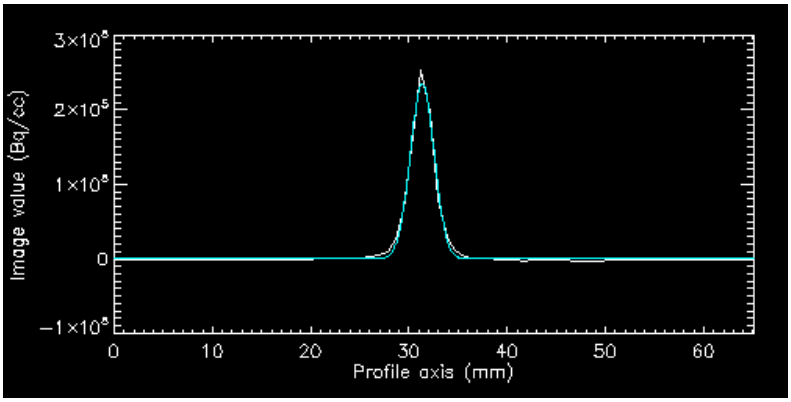

Figure 26. Profile from spatial resolution measurement with FBP of Figure 25, i.e. ^{89}Zr 38 mm off-axis. FWHM from this profile is depicted in Figure 27.

The resolution measurements of ^{89}Zr were compared to ^{18}F. The results are summarised below in Figure 27 and Figure 28. The two pictures represent different reconstruction algorithms.

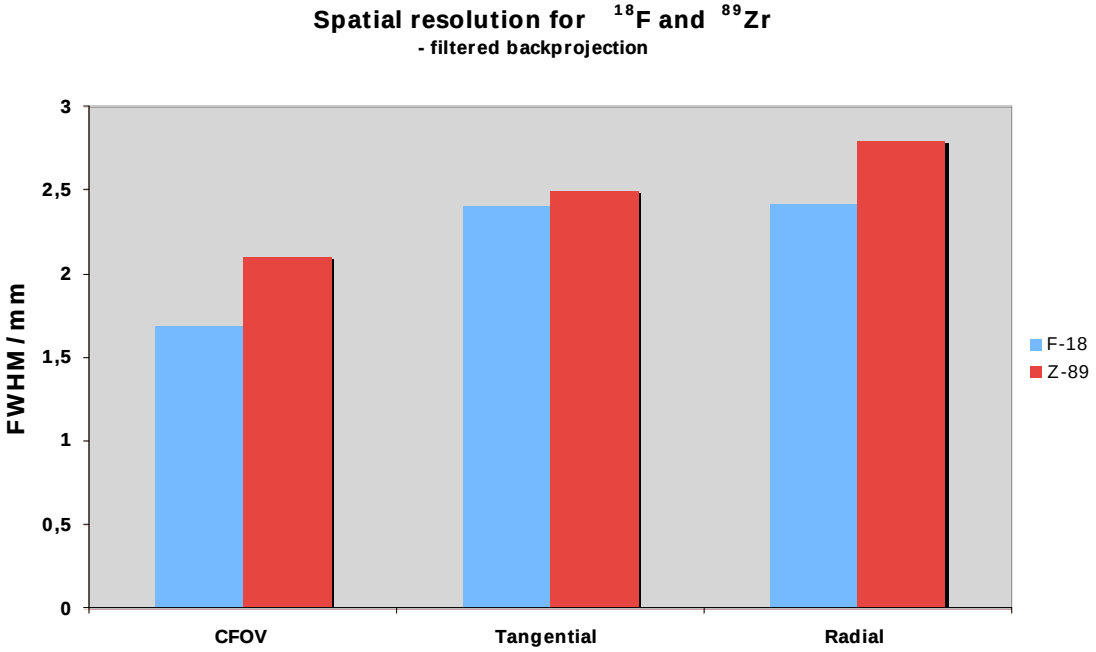

Figure 27. Spatial resolution of ^{18}F vs. ^{89}Zr with filtered backprojection. Measurements in the three positions: CFOV, 28 mm tangential of CFOV and 38 mm radial of CFOV. Refer to Figure 15.

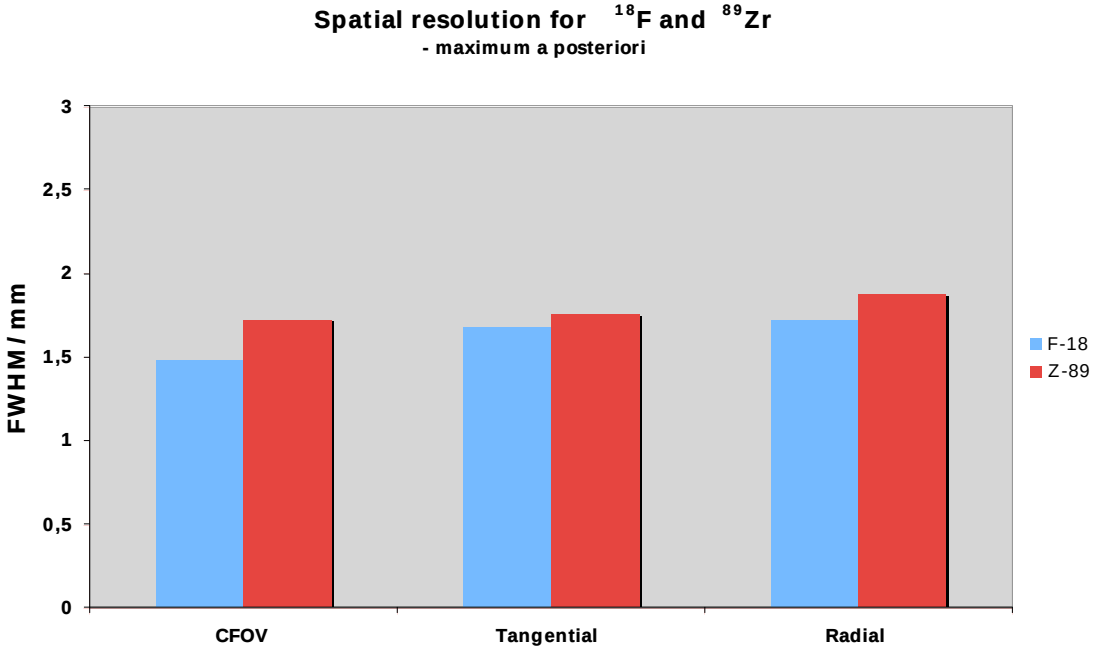

Figure 28. Comparison of spatial resolution between ^{18}F and ^{89}Zr with maximum posteriori (MAP). Measurements in three positions: CFOV, 28 mm tangential of CFOV and 38 mm radial of CFOV. Refer to Figure 15.

4.4.2 Sensitivity

Due to an unexpected behaviour of the radioactive solution, results from the sensitivity measurements in the MicroPET Focus 120 were not obtainable. Added sodium permanganate that precipitated destroyed the homogeneity of the phantom. The sensitivity experiments were repeated in GE 4096 *Plus* and the following results derive from measurements in this camera. Again, the measurements are relative ^{18}F.

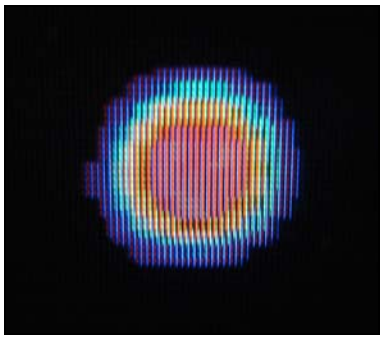

Figure 29. Reconstructed image of a sensitivity measurement of ^{89}Zr in a whole body PET scanner (GE 4096 *Plus*).

In Table 2 the activity ratios of ^{18}F and ^{89}Zr are measured in an ion-chamber and compared to the ratios measured in Ge 4096 *Plus*.

Table 2. Results from a relative sensitivity measurement of ^{89}Zr to ^{18}F in GE 4096 *Plus*. $Mean_{corr}$ (nCi/ml) is corrected for the positron abundance per decay (22.4 % for ^{89}Zr and 96.7 % for ^{18}F). Activities are measured in the ion-chamber (Capintec CRC-5RB), while "Mean(nCi/ml)" are measured in GE 4096 *Plus*.

Nuclide	Activity (A) (MBq/ml)	Mean* (nCi/ml)	$Mean_{corr}$ ** (M_{corr}) (nCi/ml)	$M_{corr(18F)}/M_{corr(89Zr)}$	$A(^{18}F)/A(^{89}Zr)$
F-18	0,034	618	658	**0,15**	**0,15**
Zr-89	0,23	980	4395		

* ROI placed in the third slice

** ^{18}F is corrected for decay during measurement as well

4.4.3 Scatter

Figure 30 below depicts reconstructed images of the scatter phantom (refer Figure 19) filled with ^{18}F and ^{89}Zr, respectively. The images reveal a pretty good activity distribution within the phantom, and in the middle the cold spot is shown. Through the phantom a profile line was drawn (red straight line) and the activity along this line is depicted in the same image (red line with two peaks).

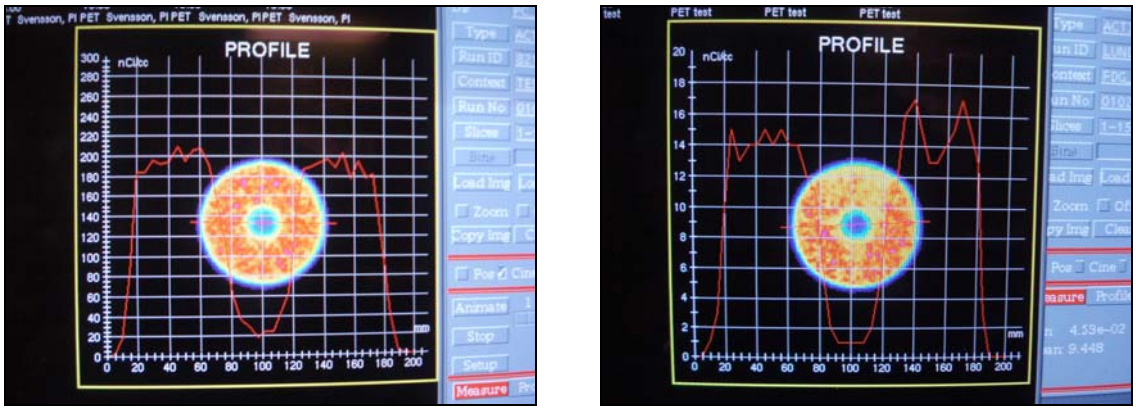

Figure 30. Reconstructed images of ^{18}F (left) and ^{89}Zr (right). A profile through the phantom shows the activity distribution.

The scatter contribution for ^{18}F is approximately 10 % (20/200) and 7 % (1/14) for ^{89}Zr. This indicates no extra contribution from the 909 keV gammas emitted in coincidence with 511 keV annihilation photons in ^{89}Zr.

5 Discussion

Until the beginning of this thesis no work has been done on ^{89}Zr at Lund University and no publications from the rest of Scandinavia have been found. This concerns both the production, separation, conjugation and phantom, animal or clinical studies. Globally, little effort has been put into this radionuclide that makes this an even more interesting research area. In this thesis, much work has consisted of building up the laboratory and to repeat the work done by Verel *et al.* I have tried to deal with those problems met during this thesis as good as possible, but some resulted in a significant time delay that caused the exclusion of planned investigations. Also time for repeated measurements was limited.

5.1 Production

The results from γ-spectroscopy verified that ^{89}Zr has been produced as well as ^{88}Zr and ^{89m}Zr. Verel *et al.* measured a quantity of 0.00015% ^{88}Zr (irradiation with 14 MeV protons, 65-80 μA, 2-3 h). Even though no quantification of ^{88}Zr has been done, the yield of this radionuclide might be higher since 16 MeV protons (~16 μA, 1 h) compared to 14 MeV activated the Y-foil. Regarding Figure 4, an increase of proton energy from 14 to 16 MeV leads to approximately 3-400-fold increase of the cross section for the reaction ^{89}Y(p,2n)^{88}Zr.

Since no measurements longer than 10 min were performed, the activated impurities from the Y-foil found by Verel *et al.* (^{48}V, ^{56}Co, and ^{156}Tb) were not revealed. Anyhow, if these radionuclidic impurities have been co-produced, they should have been excluded in the separation process. The large amount of ^{89m}Zr ($T_{½}$ = 4 min) very close to EOB suggests that the irradiated foil should rest at the cyclotron for at least 1 h before separation, to avoid unnecessary radiation exposure.

It was found from the quantification that absence of ^{89m}Zr was important since it positron decays (6%) and thus affects the quantification. The relative quantification with γ-spectroscopy was made with a large source-detector distance that eliminated a geometry dependence of the ^{18}F and ^{89}Zr samples. However, a slightly difference in radioactivity was observed when measuring on an intact foil compared to a dissolved foil of ^{89}Zr, which indicates a small geometry dependence of the ion chamber Capintec CRC-5RB.

5.2 Separation

Four separations have been carried out that resulted in overall radiochemical yields of 84, 83, 94 and 85 % respectively. This should be compared to the yields by Verel *et al.*, where as high as 97% was separated in five elutions of 40, 40, 10, 5 and 2% per fraction. In the first separation (yield: 84%), insufficient control over the pH during the production of the hydroxamate column mass might be the factor that decreased the amount of ^{89}Zr eluted in oxalic acid. Before the second separation the amount of EDC was adjusted as well as the concentration of NaOH, which was found to be too weak. However, this adjustment was found to not increase the overall yield of separated ^{89}Zr (yield: 83%). In the second separation in Figure 21, one can see that the first elution is low (18%) compared to the others (36% and 32%). An explanation for this might be

that air has been introduced into the tubes, which could have resulted in a reduced volume of oxalic acid washed through the column. The following elutions resulted in high yields, and especially in the last elution where #5 contributed with 7% to overall yield (compare 1% and 3% respectively). When measuring on the column, 9% of the activity was found to be left, that indicates a failure in the first elution. The third separation was the most successful. A well produced column mass with an additional two elutions (total 7 elutions) gave a radiochemical yield of 94%. In this separation the starting activity (i.e. dissolved foil) was higher, which is a more convenient amount of radioactivity for the ion chamber. The ion chamber might be more inaccurate for low activity levels.

A further modification of the production of hydroxamate column mass has been tried. Instead of washing the column mass through a funnel, the last washing was done by shaking and decanting, shaking decanting etc. This might lead to a better exclusion of the different urea products from different reactions. The hydroxamate column mass was stored in argon conditions after freeze-drying to prevent reactions of humid air. However, the fourth separation yielded "only" 85 %. The first elution is very low (12 %) compared to the others. The rest of the elutions in this separation were very effective that indicated some kind of failure in the first elution. A suggestion should be the use of vacutainers with larger volume to eliminate the extra introduction air to the system. This together with a larger amount of column mass (> 100mg) might lead to higher yields.

In the beginning, to test the experimental routines a non-radioactive Y-foil was dissolved in HCl. The foil was completely dissolved after 2 ml 1M HCl and a clear solution was achieved. Surprisingly, when dissolving a radioactive foil a couple of weeks later the behaviour was not the same. The foil was not dissolved before 12M HCl was added and the solution turned out grey. The manufacturer deliver the Y-foil in argon conditions, while after opening, the foil was kept during normal atmosphere. Probably the foil has been a subject to oxidation and it is not clear whether it has affected the separation (and purity). In Figure 7 this presumed oxidation layer is clearly seen when it has stocked in the resin. It might, however, be important to keep the foil in argon conditions in the future. One could easily see that the presumed oxidation layer had adsorbed in the vial. When measuring on these vials at least 5 % of the initial radioactivity was left. A suggestion should be to add an extra washing with 2M HCl.

As mentioned above, the PIXE analysis could unfortunately not proceed due to high radioactivity levels of the ^{89}Zr samples. The radioactive ^{89}Zr contributed to a large compton background which in turn drowned the x-ray peaks that would reveal the presence of stable elements. This analysis was of crucial importance as a quality control of the hydroxamate column mass. For the moment the amount of stable impurities in the ^{89}Zr oxalate is not clear. This problem can be overcome in two ways: either await the radioactivity to disappear and count the amount of ^{89}Zr backwards or carry out the elution with a non-radioactive foil. If the ion exchange works in a satisfying way, there should be no significant amounts of impurities present in the elute of oxalic acid.

5.3 Phantom studies

The results from the phantom studies in MicroPET Focus 120 were sometimes successful, sometimes unsuccessful. With filtered backprojection a spatial resolution in CFOV from ^{18}F and ^{89}Zr was measured to 1.7 mm and 2.1 mm respectively. This means

a spatial resolution loss of 0.4 mm for ^{89}Zr, which is pretty similar the results in Table 1 (0.3 mm difference). With MAP reconstruction a better spatial resolution was measured (~1.5 mm and 1.7 mm for ^{18}F and ^{89}Zr) and a resolution loss of 0.2 mm was found for ^{89}Zr in CFOV. It is clearly seen that the best spatial resolution is obtained in CFOV and is decreased when moved away from ditto. The difference between the two radionuclides is also less pronounced as you move further away from CFOV.

Unfortunately, the sensitivity measurement in MicroPET Focus 120 with ^{89}Zr failed. Since the ^{89}Zr oxalate is a transparent solution some sodium permanganate (KMnO4) was added to colour it, to have a better control over contamination during preparation of the phantoms as well as to visualize the solutions´ homogeneity. It was found that the sodium permanganate precipitated with Zr which made the sensitivity phantom useless. The sensitivity measurement was repeated in GE 4096 *Plus* and was more successful. This experiment showed no difference in sensitivity in this scanner between ^{18}F and ^{89}Zr that indicated no impact from the 909 keV gammas from ^{89}Zr. However, from this it cannot be concluded that sensitivity of ^{89}Zr equals ^{18}F in the MicroPET Focus 120 since data are collected in 3D mode which increases the sensitivity. This might then show different sensitivity for these two radionuclides. Results from scatter measurements indicated no significant difference between ^{18}F and ^{89}Zr in GE 4096 *Plus*, i.e. no additional contribution from 909 keV gammas in ^{89}Zr. Thus, the lack of energy discrimination above 511 keV in GE 4096 *Plus* seems to be no problem.

Hence, ^{89}Zr shows similar imaging characteristics to ^{18}F (in GE 4096 *Plus*) which enables good quantification possibilities.

5.4 Conjugation

Attempts to produce TFP-*N*-sucDf-Fe have been done, i.e. the modification of Df, filled with Fe and esterfied with TFP. This synthesis contains three of the six steps in the conjugation between ^{89}Zr and the mAbs. The production yielded in 0.97 g. During the synthesis of *N*-sucDf when 12M HCl was added to lower pH to 2 (step 9, *Appendix III*) to make *N*-sucDf start precipitate, pH was accidentally lowered to 1.1. No need for adjustment is required if pH exceeds 1. Thus, this it not believed to affect the quality, but might influence the final yield. There should be no problem to achieve 1.3 g *N*-sucDf with careful decantation and a more optimized pH.

The first attempt to conjugate mAbs to ^{89}Zr turned out negative. Rituximab, in the form Rituximab-TFP-*N*-sucDf, seemed to stuck in the PD-10 column while gentisic acid was eluted. The second try of producing Rituximab-TFP-*N*-sucDf resulted in > 60 % loss of Rituximab, but was considerably better than the first attempt. It was found that the wrong kind of gentisic acid was used. Instead of gentisic acid, gentisic acid sodium salt hydrate was utilized. This was discovered during the preparation of “gentisic acid 5 mg/ml” and “gentisic acid 100 mg/ml” when pH was completely out of range of the expected. Even though the pH was adjusted with 0.1 M Na_2CO_3, this additional sodium salt hydrate might violate the fundamental chemistry. The lack of time prevented further productions. For the labelling of ^{89}Zr it was found that HEPES did not act as that strong indifferent buffer at pH 7.2-7.4 as required, namely this narrow range of pH where ^{89}Zr oxalate is able to be transchelated into Rituximab-TFP-*N*-sucDf. This in combination with wrong kind of gentisic acid might be the cause of the unsuccessful labelling of ^{89}Zr to Rituximab.

6 Conclusions

Below, the purpose scheme from the beginning is depicted to sum up the successful outcomes of this thesis. ^{89}Zr has been produced and separated to a radiochemical yield ≥ 83 %. Due to problem with PIXE analysis the amount of stable impurities in ^{89}Zr oxalate could not be investigated. It is therefore not clear whether the presumed oxidation of the Y-foil has had any affect in the separation step. It is suggested to do the separation chemistry on a non-radioactive foil to overcome this problem.

Due to the lack of time no further attempts to conjugate Rituximab to ^{89}Zr were done. A future suggestion is to use gentisic acid instead of gentisic acid sodium salt hydrate. Better control over pH for the HEPES solution is also very important.

Phantom studies showed a spatial resolution loss of 0.3 mm (FBP) for ^{89}Zr compared to ^{18}F in the MicroPET Focus 120. In GE 4096 *Plus*, equal sensitivity and no extra scatter contribution from 909 keV gammas in ^{89}Zr was seen. This indicates very good imaging characteristics of ^{89}Zr.

Even though the conjugation was not successful in the scope of this thesis, there is still hope to conjugate mAbs against PSA and hK2 in the development of radioimmunodiagnostics of prostate cancer.
To reach the final goal of animal and clinical studies, the most important steps in this moment is:

- Investigation of stable impurities in ^{89}Zr oxalate
- Manage a successful conjugation ^{89}Zr to Rituximab
- Conjugation of mAbs against PSA and/or hK2

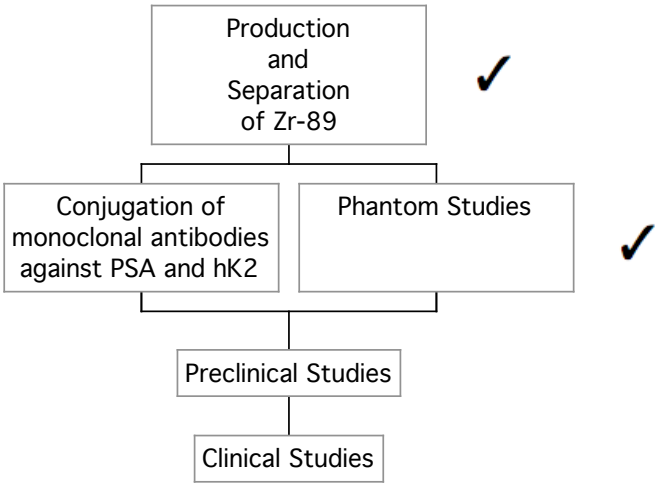

7 References

1. Eary, J.F., *Fundamentals of radioimmunotherapy.* Int J Rad Appl Instrum B, 1991. **18**(1): p. 105-8.
2. Barbet, J., et al., *Which radionuclides will nuclear oncology need tomorrow?* Eur J Nucl Med Mol Imaging, 2006. **33**(6): p. 627-30.
3. Borjesson, P.K., et al., *Performance of immuno-positron emission tomography with zirconium-89-labeled chimeric monoclonal antibody U36 in the detection of lymph node metastases in head and neck cancer patients.* Clin Cancer Res, 2006. **12**(7 Pt 1): p. 2133-40.
4. Massoud, T.F. and S.S. Gambhir, *Molecular imaging in living subjects: seeing fundamental biological processes in a new light.* Genes Dev, 2003. **17**(5): p. 545-80.
5. Ulmert, D., *Assessments of PSA-forms and hK2 as very early predictors of prostate cancer*. 2007. 13-27.
6. Cancerfonden, *Cancerfondsrapporten.* 2007.
7. Cancerfonden, *Om prostatacancer*. 2005.
8. Malm, J. and H. Lilja, *Biochemistry of prostate specific antigen, PSA.* Scand J Clin Lab Invest Suppl, 1995. **221**: p. 15-22.
9. Stege, R.H., et al., *Tissue PSA from fine-needle biopsies of prostatic carcinoma as related to serum PSA, clinical stage, cytological grade, and DNA ploidy.* Prostate, 1999. **38**(3): p. 183-8.
10. Björk, T., *PSA - Prostata-Specifikt Antigen.* Incitament, 2006(1): p. 31-34.
11. Lintula, S., et al., *Relative concentrations of hK2/PSA mRNA in benign and malignant prostatic tissue.* Prostate, 2005. **63**(4): p. 324-9.
12. Becker, C., et al., *Testing in serum for human glandular kallikrein 2, and free and total prostate specific antigen in biannual screening for prostate cancer.* J Urol, 2003. **170**(4 Pt 1): p. 1169-74.
13. Darson, M.F., et al., *Human glandular kallikrein 2 expression in prostate adenocarcinoma and lymph node metastases.* Urology, 1999. **53**(5): p. 939-44.
14. Hans Lundqvist, M.L., Vladimir Tolmachev, *Positron Emission Tomography.* Eur J Phys, 1998. **19**: p. 537-552.
15. Phelps, M.E., *PET Molecular Imaging and its Biological Applications*. 9 ed. 2004, New York: Springer. p. 3-10.
16. Miles N. Wernick, J.N.A., ed. *Emission Tomography: The Fundamentals of PET and SPECT*. 2004, Elsevier Inc. 179-181.
17. Verel, I., G.W. Visser, and G.A. van Dongen, *The promise of immuno-PET in radioimmunotherapy.* J Nucl Med, 2005. **46 Suppl 1**: p. 164S-71S.
18. M.A. Miller, N.C.R., G.d. Hutchins. *SMALL ANIMAL PET IMAGING.* in *ASTROPARTICLE, PARTICLE AND SPACE PHYSICS, DETECTORS AND MEDICAL PHYSICS APPLICATIONS Proceedings of the 8th Conference.* 2003. Villa Olmo, Como, Italy.
19. Chatziioannou, A.F., *PET scanners dedicated to molecular imaging of small animal models.* Mol Imaging Biol, 2002. **4**(1): p. 47-63.
20. Myers, R. and S. Hume, *Small animal PET.* Eur Neuropsychopharmacol, 2002. **12**(6): p. 545-55.
21. Wang, Z., *Radioimmunotherapy and Extracorporeal Adsorption.* 2005.

22. Meijs, W.E., et al., *Zirconium-labeled monoclonal antibodies and their distribution in tumor-bearing nude mice.* J Nucl Med, 1997. **38**(1): p. 112-8.
23. Lundqvist, H. and V. Tolmachev, *Targeting peptides and positron emission tomography.* Biopolymers, 2002. **66**(6): p. 381-92.
24. Verel, I., et al., *89Zr immuno-PET: comprehensive procedures for the production of 89Zr-labeled monoclonal antibodies.* J Nucl Med, 2003. **44**(8): p. 1271-81.
25. Pagani, M.S.-E., Sharon; Larsson, Stig A., *Alternative positron emission tomography with non-conventional positron emitters: effects of their physical properties on image quality and potential clinical applications.* European Journal of Nuclear Medicine, 1997. **24**(10): p. 1301-1327.
26. Lee, F.T. and A.M.i. Scott, *Immuno-PET for tumor targeting.* J Nucl Med, 2003. **44**(8): p. 1282-3.
27. Ekman, A., in *Nationalencyklopedien*. 1996, Bra Böcker: Höganäs. p. 301-302.
28. O.T. Dejesus, R.J.N., *Production and Purification of 89Zr, a Potential PET Antibody Label.* Appl. Radiat. Isot., 1990. **41**(8): p. 789-790.
29. Kandil, S., et al., *A comparative study on the separation of radiozirconium via ion-exchange and solvent extraction techniques, with particular reference to the production of 88Zr and 89Zr in proton induced reactions on yttrium.* Journal of Radioanalytical and Nuclear Chemistry, 2007. **274**(1): p. 1-8.
30. Kalman Shure, M.D., *Radiations from Zr89* Physical Review, 1951. **82**(1): p. 122-122.
31. Verel, I., et al., *Quantitative 89Zr immuno-PET for in vivo scouting of 90Y-labeled monoclonal antibodies in xenograft-bearing nude mice.* J Nucl Med, 2003. **44**(10): p. 1663-70.
32. Wilma E. Meijs, J.D.M.H., Hiddie J. Haisma, et al. issn *Production of Highly Pure No-carrier Added 89Zr for the Labelling of Antibodies with a Positron Emitter.* Appl. Radiat. Isot., 1994. **45**(12): p. 1143-1147.
33. Richard B. Firestone, V.S.S., Coral M. Baglin, S.Y. Frank Chu, and Jean Zipkin, *Table of isotopes*. 1999, John Wiley & Sons, Inc.: New York.
34. Mustafa, M.G., et al., *Measurements and a direct-reaction–plus–Hauser-Feshbach analysis of^{89}Y(p,n)^{89}Zr,^{89}Y(p,2n)^{88}, and^{89}Y(p,pn)^{88}Y reactions up to 40 MeV.* Physical Review C, 1988. **38**(4): p. 1624.
35. J. Zweit, S.D., H.L. Sharma, *Production of No-carrier added Zirconium-89 for Positron Emission Tomography.* Appl. Radiat. Isot., 1991. **42**(2): p. 199-201.
36. Richard J. Kowalsky, S.W.F., *Radiopharmaceuticals in Nuclear Pharmacy and Nuclear Medicine.* 2 ed. 2004: American Pharmacists Association (APhA). 258-260, 405-407.
37. Meijs, W.E., et al., *Evaluation of desferal as a bifunctional chelating agent for labeling antibodies with Zr-89.* Int J Rad Appl Instrum [A], 1992. **43**(12): p. 1443-7.
38. Krane, K.S., *Introductory Nuclear Physics.* 30 ed. 1988: John Wiley & Sons. 791-792.
39. Kärnfysik. *Välkommen till mikrostrålelaboratoriet i Lund.* [cited; Available from: http://micro.pixe.lth.se/English/research_med.htm.
40. Fysikum. *PIXE, particle induced x-ray emission, 2007.* 2007 [cited; Available from: http://jack.pixe.lth.se/kfgu/AccMetoder/Projects/PIXE_LAB.pdf.
41. Jönsson, J.Å., in *Nationalencyklopedin*. 1993, Bra Böcker. p. 461.

42. Kim, J.S., et al., *Performance measurement of the microPET focus 120 scanner.* J Nucl Med, 2007. **48**(9): p. 1527-35.

Appendix I

Protokoll för framställning av hydroxamatkolonnmassa

Datum:

Syfte

I detta protokoll avses framställning av hydroxamatkolonnmassa, som är en modifiering av Accel Plus katjonbytarmassa. Kolonnmassan används för separering av ^{89}Zr från en bestrålad ^{89}Y-folie.

Material

Produktinformation för kemikalier i detta protokoll återfinns i *Produktbilaga A*. För information om aktuell tillredning av lösningar hänvisas till *Referens.*

Lösning/kemikalie	**Referens**
1 g Accel Plus CM	
148 ml injektionsvatten	
180 µl 3 M HCl	
2 ml TFP-lösning (200 mg/ml i MeCN, 1.2 mmol)	
768 mg EDC (2 mmol)	
2 ml 1 M NaOH	
690 mg hydroxylamin hydroklorid (10 mmol)	

Förbrukningsmaterial

Pipettips 1000 µl
Pipettips 200 µl
Falconrör, 50 ml
Filter (sköljningstratt)
Tungspatlar
Kleenexservetter
Scintillationsburkar
Vågpapper
Aluminiumfolie

Materiel

Pipett 100-1000 µl
Pipett 40-200 µl
Våg
pH-utrustning (elektrod med protelyt elektrolyt, kalibreringsbuffrar)

Trefot med hållare
Vagga (Hotlab)
Frys
Vakuumpump (Büchi Vacuum Pump V700, Vacuum Controller V-850)
Tratt

Steg 1 – Esterfiering av katjonbytarmassan

För att erhålla en hög andel av de tillsatta hydroxamatgrupper i kolonnmassan, esterfieras karboxylsyragrupperna i katjonbytarmassan. Detta utföres i två steg för en optimal esterfiering.

1. Kalibrera pH-mätaren.

2. Väg upp 1 g (±0.01 g) Accell Plus CM i ett falconrör.

   Vikt:_____

3. Suspendera katjonbytarmassan i 8 mL "injektionsvatten" och blanda väl.

Tillsätt därefter:

4. 75 µL 3M HCl

5. 1 mL TFP-lösning (200 mg/mL i MeCN, 1.2 mmol)

6. Väg därefter upp 384 mg (± 4mg) EDC (2 mmol) på ett "halt" papper och tillsätt lösningen.

   Vikt:_____

7. Mät pH (acceptansintervall: 5.7-6.0)

   pH =_____

8. Mixa 1h i "vaggan" på Hotlab. (OBS! Falconrör passar ej perfekt i vaggan. Använd en bit tejp för att fästa röret.)

Tillsätt på nytt:

9. 105 µL 3M HCl

10. 1 mL TFP-lösning

11. Väg därefter upp 384 mg (± 4mg) EDC (2 mmol) på ett "halt" papper och tillsätt lösningen.

    Vikt:_____

12. Mät pH (acceptansintervall 5.7-6.0)

    pH =_____

I fall pH är för högt - justera med 3M HCl
I fall pH är för lågt - justera med EDC

13. Mixa 1h i "vaggan" på Hotlab.

14. För över lösningen till en tratt (inkl. filter) och skölj med 30 mL MeCN. Låt filterpappret torka > 20 min så att det inte är genomvått.

Under tiden gå vidare till steg 2.

Steg 2 – Introducering av hydroxamatgrupper

1. Förbered hydroxylaminhydrokloridlösningen i ett nytt falconrör genom:

    a. 1 mL 1M NaOH + 2 mL MeOH

    b. Väg upp 690 mg (10 mmol) hydroxylamine hydrochloride m.h.a. Al-folie och tillsätt lösningen.

        Vikt:_____

    c. Efter 5 min, tillsätt 1 mL 1M NaOH

    d. Mät pH (acceptansintervall 5.3-5.4)

        pH =_____

2. Skrapa försiktigt bort det återstående pulvret från filtreringen i punkt 12 med en tungspatel.
   OBS! Skrapa inte för djupt så att filterpappret rivs upp! Tillsätt till hydroxylaminhydrokloridlösningen.

3. Mät pH (acceptansintervall: 5.1-5.2)

   pH =_____

4. Mixa över natten i rumstemperatur i "vaggan" på Hotlab

5. För över lösningen till en tratt (inkl. filter).

6. Skölj kolonnmaterialet med 140 mL ”injektionsvatten” och 70 mL MeCN

7. För över filterpappret till en aluminiumform och förvara i frysen över natten.

8. Frystorka i vakuumpumpen vid cyclotronen. Tid: 3h

9. Märk en scintillationsburk med "Hydroxamatkolonnmassa" samt datum. Tarera därefter en våg med burken på.

10. Skrapa försiktigt av katjonbytarmassan m.h.a. en tungspatel. Undvik att skrapa för djupt i pappret!
    För över kolonnmassan till scinitallationsburken och väg.

    Vikt:_____

Materialet kan härifrån förvaras upp till 4 månader

Produktbilaga A

Kvantiteter av nedanstående kemikalier hänvisas till protokollet.

Produkt	**Namn**	**CAS-nr**	**LOT**	**Produktnr**	**Tillverkare**
Accel Plus CM	Accel Plus CM Cation Exchange Media 300Å		040B	WAT010740	Waters
HCl	Saltsyra	7647-01-0	70540	30721-1L	Sigma-Aldrich
TFP	2,3,5,6-Tetraflurophenol, 98%	769-39-1	A0239446	162-188395	Acros Organics
EDC	1-(3-Dimethylaminopropyl)-3-ethylcarbodiimide hydrochloride	25952-53-8	A0240928	171440100	Acros Organics
NaOH	natriumhydroxid	1310-73-2	B849795 631	1.06495.0250	VWR
hydroxylamine hydroklorid		5470-11-1	05310DH (?)	379921	Sigma-Aldrich

Appendix II

Protokoll för separering av ^{89}Zr

Datum:

Syfte

Efter bestrålning av ^{89}Y-folie i cyclotron, löses folien i HCl. Denna lösning får sedan passera genom en hydroxamatkolonn för att avlägsna föroreningar för att sedan skölja ut ^{89}Zr med hjälp av oxalsyra. ^{89}Zr kommer således befinna sig i en oxalsyralösning.

Material

Produktinformation för kemikalier i detta protokoll återfinns i *Produktbilaga B*. För information om aktuell tillredning av lösningar hänvisas till *Referens.*

Lösning/kemikalie	**Referens**
~10 ml 1 M HCl	
100 µl väteperxoid	
0.22 ml 12 M HCl	
100 mg hydroxamatkolonnmassa	Se protokoll
12 ml 0.9 % NaCl	
5 ml MeCN	
8 ml 2M HCl	
6 ml injektionsvatten (sterilt vatten)	
2.5 ml oxalsyra	

Förbrukningsmaterial
Pipettips 1000 µl
Pipettips 200 µl
Falconrör, 50 ml
Filter (sköljningstratt)
Tungspatlar
Kleenexservetter
Scintillationsburkar
Vågpapper
Aluminiumfolie
Kanyl
Extract Clean tube plus filter
Engångspipett
Vacutainerrör, 1.5 ml
Provväxlarrör (röd kork)

Materiel
Pipett 100-1000 µl
Pipett 40-200 µl

Bägare
Våg
Aktivetsmätare (jonkammare)
Uppställning för kolonn

Steg 1 – Lösa upp target

1. Märk följande provrör

Provrörstyp	Namn
Falconrör	*Target*
	Sköljrest I
	Y-eluat II
	Kolonn
Vacutainerrör	*Y-eluat I*
	#1
	#2
	#3
	#4
	#5

2. Mät den bestrålade folien i aktivitetsmätaren (typ). Se till så att rätt radionuklid är inställd.

A_{folie} = _____

kl. _____

datum:_____

3. Placera folien i ett falconrör märkt "Target"

4. Lös folien sakta successivt i 4*0.5 mL 1M HCl i ett falconrör.

5. Tag fram väteperoxid ur kylskåpet i kaninlabbet

6. Tillsätt 0.1 mL väteperoxid (H2O2) för att oxidera till Zr(IV). Viktigt vid transkelering till desferal.

7. Ställ tillbaka väteperoxiden i kylskåpet

8. Tillsätt 0.22 mL 12M HCl för att erhålla en slutlig koncentration av 2M HCl

9. Placera falconröret bakom blyskydd.

10. Vänta 1 h

11. Mät aktiviteten igen

$A_{folie, HCl}$ = _____

kl. _____

datum:_____

Steg 2 – Förberedelse av hydroxamatkolonnen och eluering

1. Placera filter i en Extract Clean tube och anslut till uppställningen. Applicera en kanyl (grå) på kolonnen.

2. Som kontroll över att slangar och kopplingar håller tätt samt rengöring av systemet - skölj igenom med 1M HCl.
   Samla upp sköljvätskan i en bägare.

3. Väg upp 100 mg av hydroxamatkolonnmassan i ett provväxlarprovrör (röd kork)

m = _____

4. Suspendera kolonnmassan i en 1 mL 0.9% NaCl. Blanda väl!

5. Pipettera 100 µL 0.9% NaCl i den tomma kolonnen.

6. Sug upp den suspenderade kolonnmassan m.h.a. en engångspipett. Se till så att lösningen är väl blandad!
   Pipettera i kolonnen.

7. Placera ett falconrör märkt "Sköljrest I" under kolonnen. Ställ ventilen på kl. 3.

8. Skölj kolonnen genom sprutan med:

    1. 5 mL MeCN
    2. 10 mL 0.9% NaCl
    3. 2 mL 2M HCl

Vi nästföljande steg var noggrann så att verkligen all vätska sköljs igenom. Skulle av någon anledning vacutainerrören luftfyllas utan fullständigt uppsug kan vattensugen kopplas på. Vid eluering av föroreningarna är detta inte av någon vikt. Gäller främst vid elueringen av Zr.

9. Ställ ventilen på kl. 12 och ta bort falconröret "Sköljrest I". Plocka fram 89Zr-lösningen.

10. Koppla slangen till 89Zr-lösningen och initiera med med vacutainerröet "Y-eluat".
    Märk röret även med tid och datum.

11. Avlägsna vacutainerröet och ställ ventilen på kl. 3.

12. Placera falconröret märkt "Y-eluat II" under kanylen.

13. Skölj kolonnen med 6 mL 2M HCl och 6 mL sterilt ”injektionsvatten”.

14. Ställ bort falconröret och vrid ventilen till kl. 12.

15. Tag ett nytt falconrör och pipettera 0.5 mL 1M oxalsyra. Initiera Zr-elueringen med vacutainerrör "#1".
    Upprepa proceduren tills 5 portioner erhållits.
    Rören skall dessutom vara märkta med: radionuklid
    tid
    datum

16. Avlägsna kolonn+kanyl och placera i ett falconrör märkt "Kolonn".

17. Mät därefter de fem Zr-portionerna, Y-eluat I-II samt Kolonn. Märk rören dessutom med radionuklid, aktivitet, klockslag och datum.

Prov	**Aktivitet (MBq)**	**Klockslag och datum**
#1		
#2		
#3		
#4		
#5		
Delsumma:		
Y-eluat I		
Y-eluat II		
Kolonn		
Target		
Summa:		
$A_{folie, HCl}$[4]:		

[4] Korrigera för sönderfall i fall det gått längre tid än 1 h.

Produktbilaga B

Kvantiteter av nedanstående kemikalier hänvisas till protokollet.

Produkt	Namn	CAS-nr	LOT	Produktnr	Tillverkare
HCl	Saltsyra	7647-01-0	70540	30721-1L	Sigma-Aldrich
H_2O_2	Väteperoxid (30 %)	7722-84-1	076K34641	21676-3	Sigma-Aldrich
MeCN	Acetonitril CHROMASOLV for HPLC, gradient grade (metylcyanid)		7134A	34851	Sigma-Aldrich
Oxalsyra		144-62-7	08723AH-207	19413-1	Sigma-Aldrich
Extract clean tube				52.5122381	ScantecLab
Frits for 1.5 ml SPE Reservoir 100pk				52.2106739	ScantecLab
Vacutainer	Hemogard 5ml utan tillsats		7176167	367614	BD

Appendix III

Protokoll inför konjugering av ^{89}Zr till mAb

- framställning av *N*-sucDf-Fe
-

Datum:

Syfte

Protokollet avser att framställa esterfierat desferal blockerat med Fe(III), *N*-sucDf-Fe, inför konjugering mot monoklonala antikroppar samt märkning med ^{89}Zr.

Material

Produktinformation för kemikalier i detta protokoll återfinns i *Produktbilaga C.* För information om aktuell tillredning av lösningar hänvisas till *Referens.*

Lösningar

2.5 g Df
8.5 g bärnstenssyraanhydrid (succinic anhydride)
37.5 mL pyridine
300 mL 0.30 M NaOH
12 M HCl
0.01 HCl (iskall)
60 µL 0.1 Na_2CO_3 (plus ev. volym för pH-justering)
3 mL 0.9 % NaCl
300 µL $FeCl_3$-lösning (8 mg/mL i 0.1 M HCl)
300 µL TFP-lösning (200 mg/mL i MeCN)
120 mg EDC
11.5 mL MeCN
11 mL injektionsvatten
500 mL 0.01 M HCl

Utrustning

magnetomrörare
omrörnings- och värmeutrsutning
pH-utrustning
kyl (4 °C)
tratt
vakuumpump
frys (-70 °C)
bägare >120 m

Förbrukningsmaterial
tungspatlar
filter
Sep-Pak C_{18}
Corning® 2mL Internal Threaded Polypropylene Cryogenic Vial, Self-Standing with Round Bottom (Product #431386) (~30 st)
Parafilm
Spruta (10 ml)
Kanyl
Falconrör (50 ml)

Steg 1 – Syntes av N-sucDf

1. Tag av korkarna på Df-flaskorna m.h.a. en tång (finns i Hotlab). Gröp ur 2.5 g Df och häll i en bägare.

   m = _____

2. Väg upp 8.5 g bärnstenssyraanhydrid (succinic anhydride) på en bit Al-folie.

   m = _____

3. Häll upp 37.5 mL pyridine i en ny bägare

4. Tillsätt succinic anhydride till pyridine. Rör om.

5. Häll sedan lösningen till bägaren med Df.

6. Placera bägaren i magnetomröraren under 24 h i rumstemperatur.

   Starttid:_____

   Stopptid:_____

7. Under omrörning, tillsätt 300 mL 0.30 M NaOH för att konvertera överskottet av succinic anhydride till succinicsyra (bärnstenssyra).

8. Vänta 2 h.

9. Fortfarande under omrörning – tillsätt sakta 20-30 ml 12 M HCl för sänka pH till ca 2. Därefter i mindre volymer. Undvik att sänka pH till *under* 1, men om

detta råkas göras justera pH m.h.a. Na_2CO_3 (inte med NaOH!) . Vid detta tillfälle skall det vita N-suc Df börja så smått att fälla ut.

pH	µL
	0

10. Sätt parafilm över bägaren och placera i kylskåp till nästa dag (~16 h).

Starttid:_____

Stopptid:_____

11. Tag fram 0.01 M HCl ur frysen.

12. För att skölja bort överflödig bärnstenssyra (succinic acid) och pyridin från fällningen dekanteras lösningen, dvs. översta lagret av vätskan avlägsnas efter att fällningen ”sedimenterat”.

13. Tillsätt 0.01 M HCl till den vita produkten och skaka. Dekantera på nytt, tillsätt sedan 0.01 M HCl, skaka, osv.

14. För att kristallisera fällningen:

    i. Tillsätt ~35 mL 0.01 M HCl till den vita produkten
    ii. Värm sakta till koktemperatur under omrörningen (i kaninlabbet?)

15. Lösningen skall nu vara fullt upplöst, dvs. genomskinlig. Om inte tillsätt ~2 mL 0.01 M HCl.

16. Ta bort lösningen från värmeplattan låt den sakta svalna till rumstemperatur. Vid detta tillfälle skall kristallerna börja bildas.

17. Placera produkten så småningom i kylen över natten.

18. Tag ut lösningen från kylen och filtrera kristallerna.

19. Frystorka i vakuumpumpen vid cyclotronen. Tid: 3 h.

20. Tarera vågen vid cyclotronen efter en scintialltionsburk.

21. Skrapa över den vita produkten m.h.a. en tungspatel till scintillationsburken.

m = _____

Steg 2 – Komplexifiering av N-sucDf med Fe(III)

1. Kalibrera pH-mätaren.
2. Förbered följande lösning:
   i. Pipettera upp 60 µL 0.1 M Na_2CO_3
   ii. 3 mL 0.9 % NaCl
3. Väg upp 9 mg *N*-sucDf

   m = _____
4. Lös upp massan med lösningen från punkt 1.
5. Mät pH (acceptansintervall: 6.5-7.0)

   pH = _____

   Om lösningen är för sur, justera m.h.a. Na_2CO_3.
6. Tillsätt 300 µL av $FeCl_3$-lösning (8 mg/mL i 0.1 M HCl)
7. Vänta 10 min innan steg 3 påbörjas!

Steg 3 – Esterfiering av N-sucDf-Fe

1. Tillsätt 300 µL TFP-lösning (200 mg/mL i MeCN)
2. Tillsätt 120 mg EDC
3. Mät pH (acceptansintervall: 5.8-6.0)

   Justera m.h.a. EDC om lösningen är för sur.
4. Inkubera i 45 min.
5. Använd en spruta (10 ml) och koppla på Sep-Pak C_{18} plus lämplig kanyl.
6. Konditionera Sep-Pak C_{18} med

i. 10 mL MeCN
ii. 10 mL injektionsvatten

7. Ladda Sep-Pak C_{18} med reaktionsvolymen från (4). Lösningen, med dess karakteristiskt röda färg från Fe, skall nu fastna i ”kassetten”.

8. Skölj med 60 µL injektionsvatten

9. Eluera med 1.5 mL MeCN till ett falconrör.

10. Pipettera den eluerade lösningen till corningrör med 50 µl/rör. Ca. 30 provrör.

11. Placera provrören i frys (-70˚ C)

N-sucDf-Fe kan härifrån förvaras åtminstone i 8 veckor vid -70°C.

Produktbilaga C

Kvantiteter av nedanstående kemikalier hänvisas till protokollet.

Produkt	**Namn**	**CAS-nr**	**LOT**	**Produktnr**	**Tillverkare**
Desferal			S0520	189175	Novartis
Succinic anhydride	Bärnstenssyraanhydrid	108-86-1	1317409	239690	Aldrich
Pyridine		110-86-1	S37129-167	P5750-6	Sigma-Aldrich
NaOH	Natriumhydroxid		B849795 631	1.06495.0250	Sigma-Aldrich
HCl	Saltsyra	7647-01-0	70540		Sigma-Aldrich
Na_2CO_3	Natriumkarbonat		B208795 825	1.06395.0050	MERCK
$FeCl_3$		7705-08-0	017K3463	F7134-100G	Sigma-Aldrich
MeCN	Acetonitril CHROMASOLV for HPLC, gradient grade (metylcyanid)		7134A	34851	Sigma-Aldrich
TFP	2,3,5,6-Tetraflurophenol, 98%	769-39-1	A0239446	162-188395	Acros Organics
EDC	1-(3-Dimethylaminopropyl)-3-ethylcarbodiimide hydrochloride	25952-53-8	A0240928	171440100	Acros Organics
Sep-Pak Plus C_{18}			028637289C	WAT020515	Waters